Electronic Supplementary Material (ESI) for Inorganic Chemistry Frontiers.

Supporting Information

14-electron reduced Mo^{IV}_6-ε-Keggin polyoxometalates: highly stable and reversible electron/Li^+ sponge materials

Jie Zi[a], Meng Cao[a], Fang Yu[a,b], Cuiming Ren[a], Ruili Sang[a,b] and Li Xu*[a,b]

[a]*State Key Laboratory of Structural Chemistry, Fujian Institute of Research on the Structure of Matter, Chinese Academy of Sciences, Fuzhou 350002, Fujian, China*
[b]*Fujian College, University of Chinese Academy of Science, Fuzhou 350002, Fujian, China*
***Corresponding author.**
E-mail: xli@fjirsm.ac.cn (L. Xu)

Table of Contents

S-1 Experimental Procedures

Synthesis of precursor

Precursor $[Mo_3O_2(O_2CCH_3)_6(H_2O)_3]ZnCl_4 \cdot 8H_2O$ was prepared according to the method described in the literatures.[1, 2]

Synthesis of $[Sb_2Mo^{IV}_6Mo^{V}_2Mo^{VI}_4O_{32}(\mu_3\text{-}OH)_2py_6] \cdot 2py \cdot 2[H_2N(CH_3)_2] \cdot 1.5H_2O$ ($1 \cdot 2py \cdot 2[H_2N(CH_3)2] \cdot 1.5H_2O$, Mo^{IV}_6-POM1)

$[Mo_3O_2(O_2CCH_3)_6(H_2O)_3]ZnCl_4 \cdot 8H_2O$ (0.11 g, 0.1 mmol), Sb_2O_3 (0.01 g, 0.03 mmol) and 2-picolinic acid (Macklin, China) of 0.01g were added to a mixture solution of H_2O (2 mL), DMF (2 mL) and pyridine (7 mL). The resulting mixture was sealed in a 20 mL Teflon lined stainless-steel reactor and heated at 120 °C for 72 hours. The reactor was cooled to room temperature (25 °C) at a rate of 4 Kh^{-1} to produce black long strip crystals. Then, the products were collected and dry at the temperature of 120 °C for 12 hours under argon atmosphere. Anal. calcd for $C_{44}H_{61}Mo_{12}Sb_2N_{10}O_{35.5}$ (Mr= 2683.79): C 19.63%, H 2.28%, N 5.20%, Mo 42.75%, Sb 9.04%. Found: C 18.22%, H 2.32%, N 5.03%, Mo 37.24%, Sb 8.81%. FT-IR (KBr disc): ν = 3448 (m), 3067 (w),1608 (s), 1448 (s), 1215 (s), 1072 (s), 940 (s), 802 (s), 707 (m) and 746 (w), 563 (w) cm^{-1}.

Synthesis of $[Ge_2Mo^{IV}_6Mo^{V}_2Mo^{VI}_4O_{34}(\mu_3\text{-}OH)_2py_6] \cdot 2py \cdot 2[H_2N(CH_3)_2] \cdot 0.5H_2O$ ($2 \cdot 2Hpy \cdot 2[H_2N(CH_3)_2] \cdot 0.5H_2O$, Mo^{IV}_6-POM2)

$[Mo_3O_2(O_2CCH_3)_6(H_2O)_3]ZnCl_4 \cdot 8H_2O$ (0.11 g, 0.1 mmol), GeO_2 (0.01 g, 0.1 mmol) and 2-picolinic acid (Macklin, China) of 0.01 g were added to a mixture solution of H_2O (2 mL), DMF (2 mL) and pyridine (7 mL). The resulting mixture was sealed in a 20 mL Teflon lined stainless-steel reactor and heated at 140 °C for 72 hours. The reactor was cooled to room temperature

(25 °C) at a rate of 4 Kh^{-1} to produce black long strip crystals. Then, the products were collected and dry at the temperature of 120 °C for 12 hours under argon atmosphere. Anal. calcd for $C_{44}H_{61}Mo_{12}Ge_2N_{10}O_{36.5}$ (Mr= 2632.37): C 20.24%, H 2.36%, N 5.37%, Mo 44.10%, Ge 5.57%; Found: C 17.53%, H 2.42%, N 4.81%, Mo 42.77%, Ge 5.46%. FT-IR (KBr disc): ν = 3426 (s), 3069 (w),1609 (s), 1447 (s), 1214 (s), 1068 (s), 949 (s), 813 (s), 702 (m) and 737 (w), 540 (w) cm^{-1}.

Synthesis of $[Sb_2ZnMo^{IV}_6Mo^{V}_2Mo^{VI}_4O_{32}(\mu_3\text{-}OH)_2py_7]$ (3, Mo^{IV}_6-POM3)

$[Mo_3O_2(O_2CCH_3)_6(H_2O)_3]ZnCl_4\cdot 8H_2O$ (0.11 g, 0.1 mmol), Sb_2O_3 (0.01 g, 0.03 mmol) and 2-picolinic acid (Macklin, China) of 0.01g were added to a mixture solution of H_2O (2 mL), DMF (2 mL) and pyridine (7 mL). The resulting mixture was sealed in a 20 mL Teflon lined stainless-steel reactor and heated at 130 °C for 72 hours. Then the reactor was cooled to above 35 °C at a rate of 4 Kh^{-1} and keep the temperature for 12 hours. The platelike products were collected and dry at the temperature of 120 °C for 12 hours under argon atmosphere. Anal. calcd for $C_{35}H_{37}Mo_{12}Sb_2ZnN_7O_{34}$ (Mr= 2559.86): C 16.42%, H 1.46%, N 3.83%, Zn 2.56%, Mo 44.97%, Sb, 9.51%; Found: C 16.98%, H 1.81%, N 4.06%, Zn 2.36%, Mo 45.70%, Sb 9.07%. ν = 3450 (s), 2925 (s),1607 (s), 1448 (s), 1218 (s), 1068 (s), 948 (s), 798 (s), 705 (m) and 762 (w), 554 (w) cm^{-1}.

S-2 Materials Characterization

General: Thermogravimetric analyses (TGA) were performed on a Netzsch STA449C apparatus under N_2 flow with 10 °C/min heating. Powder X-ray diffraction (PXRD) patterns of samples were obtained on a RIGAKU MiniFlex 600 (Cu Kα radiation, λ = 1.5405 Å). Solid-state UV-vis spectra from 300 to 800 nm of powder samples were recorded on a PerkinElmer Lamda-950 UV spectrophotometer at room temperature, and $BaSO_4$ as a standard (100%

reflectance). X-ray photoelectron spectroscopy (XPS) was performed on an instrument ESCALAB 250Xi (Thermo Electron, Altrincham, U.K) with an Al Kα micro-focused X-ray source (1486 eV). IR spectra were obtained on a VERTEX70 spectrometer (Bruker Optics, America) in the range of 400-4000 cm^{-1} using KBr pellets.

The batteries with different cutoff voltages for *ex-situ* FT-IR/XPS analysis were disassembled in an argon atmosphere filled glovebox. After soaking and washing with dimethyl carbonate and drying in a glovebox for several days, the cathode was conducted the ex-situ XPS test under argon atmosphere protection. The electrodes with the same treatment were scraped off the aluminum foil and then mixed and ground with dried KBr, and the resulting mixture was pressed into sheets under a pressure of 10 K pa for *ex-situ* FT-IR test.

X-ray crystal structure analysis: Single crystal X-ray diffraction data of Mo^{IV}_6-POMs **1**-**3** were recorded on a Bruker D8-venture diffractometer with Mo-Kα radiation (λ= 0.71073 Å) equipped with a graphite monochromator. All absorption corrections were performed using multiscan. The structures were solved by direct methods and refined by full-matrix least-squares on F^2 with the SHELXTL-2016 program package. [CCDC 2246017 (**1**), CCDC 2246005 (**2**) and CCDC 2245819 (**3**) contains the supplementary crystallographic data for this paper. These data can be obtained free of charge from The Cambridge Crystallographic Data Centre via www.ccdc.cam.ac.uk/data_request/cif.].

S-3 Electrochemical measurements

The crystalline samples of **1**, **2** and **3** were dried at 120 °C under argon protection for 12 hours to remove the lattice water molecules, giving rise to the final product. The cathode material was prepared by mixing active material, acetylene black and poly (vinyl difluoride) (PVDF) binder with a weight ratio of 30: 55: 15. A suitable amount of solvent of N-methyl-2-pyrroldone

(NMP) was added into the mixture to form homogeneous slurries under vigorous stir, then pasting onto aluminum foil. The resulting cathode was dry at the temperature of 105 °C under vacuum for 12 hours. The mass loading of the active material on the Al foil is about 0.3-0.4 mg. Such a cathode, a celgard2500 separator, a lithium foil as anode and the electrolyte of 1M $LiPF_6$ in ethylene carbonate (EC)/diethyl carbonate (DEC) (1:1,v/v), were sealed into a CR2032-type coin cell in a glovebox filled with argon atmosphere for subsequent electrochemical performance measurements. Galvanostatic charge/discharge measurements, with a voltage range of 1.5-4.0 V (vs. Li/Li^+), at various current densities, were implemented on the Neware Battery testing system (NEWARE CT-4008Tn). Cyclic voltammetry (CV) curves were obtained with the electrochemical workstation (CHI 660e).

Galvanostatic intermittent titration technique (GITT) was conducted on a NEWARE CT-4008Tn instrument with current pulses of 20 minutes at a current density of 100 mA g^{-1} followed by a 40 minutes rest step. GITT was used to obtain the Li^+diffusion coefficients by the following equation[3]:

$$D_{Li} = \frac{4}{\pi\tau}\left(\frac{m_B V_M}{M_B S}\right)^2 \left(\frac{\Delta E_s}{\Delta E_t}\right)^2$$

Where D_{Li} ($cm^2\ s^{-1}$) is the chemical diffusion coefficient of Li^+; τ (s) is the constant current pulse duration; V_M ($cm^3\ mol^{-1}$), m_B (g) and M_B(g mol^{-1}) is the mole volume, mass and mole mass of active materials, respectively; S (cm^2) is the effective contact area of the electrode (herein, geometry area is adopted for estimation); ΔEs and ΔEt are the variations in the steady state voltage and overall cell voltage after applying a galvanostatic pulse in a single step GITT experiment, respectively.

Electrical conductivity measurements were performed by DC two terminal method using thin

sample pellets on a device KEITHLEY4200-SCS Semiconductor Parameter Analyzer and was referenced to the published paper[4]. The powder samples of Mo^{IV}_6-POMs**1-3** were dried at 90 °C for 10 hours under vacuum. The thin pellets were prepared by die-pressing Mo^{IV}_6-POMs**1-3** powder material with a pressure of 10 MPa. The prepared thin pellets were coated with conductive silver on both sides and electrical contacts were made using gold wires. The prepared samples were dried at 60 °C under vacuum for 5 hours and then to measure the current-voltage (I–V) characteristics. The thin pellets had a diameter of 2.5 mm and a thickness of about 1.0 mm. The bulk electrical conductivity of each material was calculated by the following equation.

$$\sigma = \frac{l \times G}{S}$$

Where σ is electrical conductivity of the sample (S cm^{-1}), l is thickness of sample (cm), S is contact area (cm^2), and G is the conductance obtained from the current versus voltage curves.

S-5 Crystallographic data

Table S1. Crystal data and structure refinement for Mo^{IV}_6-POMs**1-3**.

Compound	Mo^{IV}_6-POM**1**	Mo^{IV}_6-POM**2**	Mo^{IV}_6-POM**3**
Empirical formula	$C_{44}H_{61}Mo_{12}Sb_2N_{10}O_{35.5}$	$C_{44}H_{61}Mo_{12}Ge_2N_{10}O_{36.5}$	$C_{35}H_{37}Mo_{12}Sb_2ZnN_7O_{34}$
Formula weight	2683.79	2632.37	2559.86
Temperature	299(2) K	301(2) K	211(2) K
Wavelength	0.71073 Å	0.71073 Å	0.71073 Å
Crystal system	Orthorhombic	Orthorhombic	Monoclinic
Space group	*Cmcm*	*Cmcm*	*C* 1 2/*c* 1
Unit cell dimensions	a = 19.5638(9) Å, α= 90°. b = 26.0006(13) Å, β= 90°. c = 16.2089(8) Å, γ= 90°.	a = 19.6307(14) Å, α= 90°. b = 26.0570(16) Å, β= 90°. c = 16.3669(10) Å, γ= 90°.	a = 17.2850(8) Å, α= 90°. b = 14.7526(7) Å, b= 95.010(2)° c = 25.0511(12) Å, γ= 90°.
Volume	8245.0(7) $Å^3$	8372.0(9) $Å^3$	6363.6(5) $Å^3$
Z	4	4	4
Density (calculated)	2.206 g/cm^3	2.121 g/cm^3	2.672 g/cm^3
Absorption coefficient	2.485 mm^{-1}	2.523 mm^{-1}	3.568 mm^{-1}
F (000)	5240	5152	4816
Crystal size (mm)	0.11 x 0.04 x 0.03	0.18 x 0.05 x 0.04	0.09 x 0.08 x 0.06
θ range	2.513 to 31.047°.	3.127 to 26.766°.	2.373 to 25.714°.
Index ranges	-28 27, -34 36, -23 20	-24 24, -32 28, -20 20	-21 21, -17 17, -30 30
Reflections collected	32394	30399	28917
Independent reflections	6941	4728	6023
R (int)	0.0502	0.0415	0.0567
Completeness	99.6 %	99.2 %	99.6 %
Restraints/parameters	6934 / 131 / 281	4728 / 86 / 236	6023 / 32 / 442
S on F^2	1.028	1.041	1.088
Final R indices [I>2sigma(I)]	R_1[a] = 0.0443, wR_2[b] = 0.1194	R_1 = 0.0339, wR_2 = 0.0883	R_1 = 0.0373, wR_2 = 0.0981
R indices (all data)	R_1 = 0.0658, wR_2 = 0.1331	R_1 = 0.0374, wR_2 = 0.0909	R_1 = 0.0431, wR_2 = 0.1021

[a] $R_1=\sum||Fo|-|Fc||/\sum|Fo|$; [b] $wR_2=[\sum w(Fo^2-Fc^2)^2/\sum w(Fo^2)^2]^{1/2}$.

S-6 Structure of Mo^{IV}_6-POMs

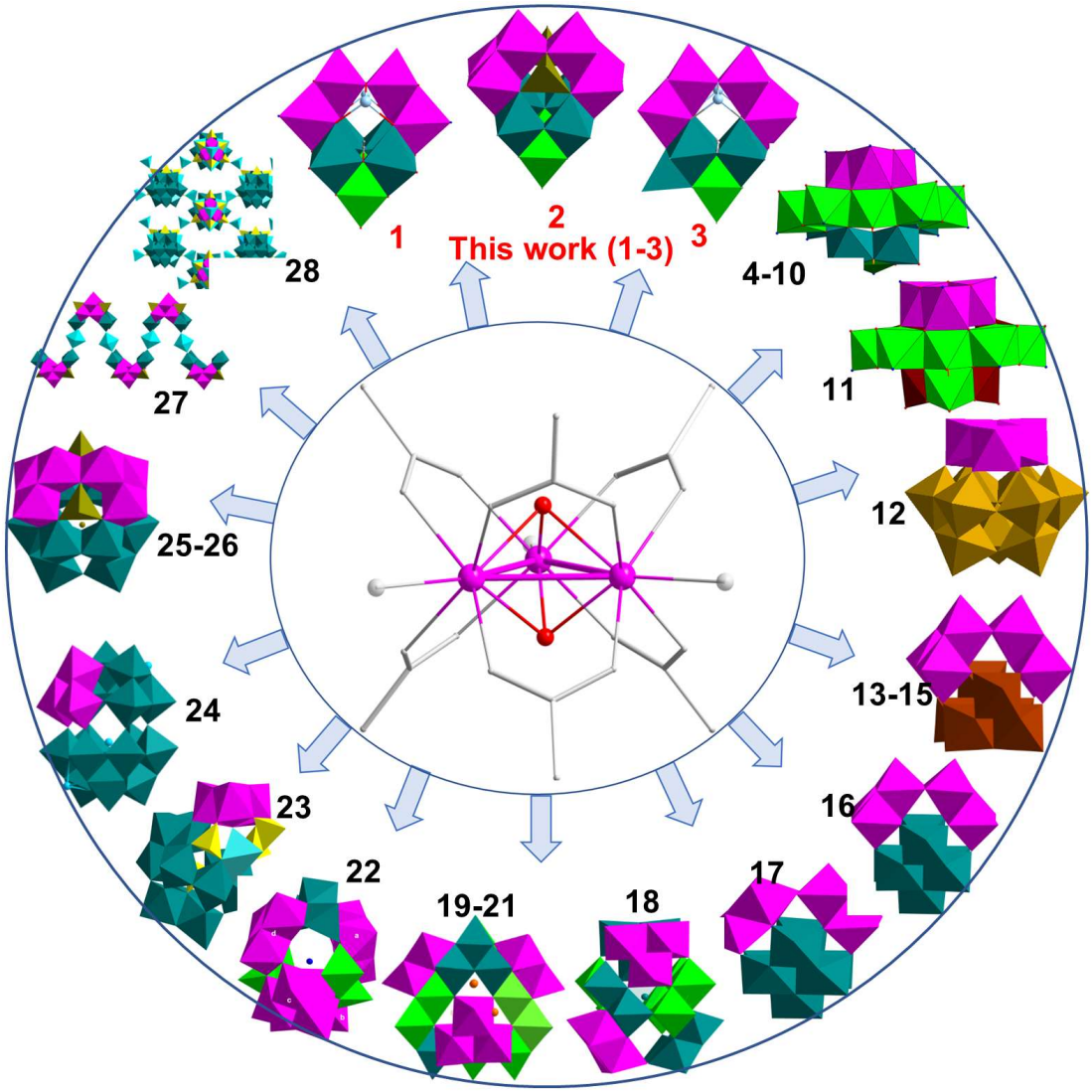

Figure S1. Polyhedral presentation of Mo^{IV}_3-POMs **1-28** (see Table S2 for corresponding compound and references) prepared from solvothermal oxidative aggregation of $[Mo^{IV}_3O_2(O_2CCH_3)_6(H_2O)_3]^{2+}$. Hydrogen atoms and pyridine molecules are omitted for clarity. Polyhedral color code: Mo^{IV}, pink; Mo^{V}, green; Mo^{VI}, teal; Mo^{VI}/W^{VI}, brown yellow; W^{6+}, brown; Ge, dark yellow; Zn, cyan; P, yellow; Atom color code: Mo, teal; Al/V, orange; Na, blue; Sb, pale blue; Ge, dark yellow.

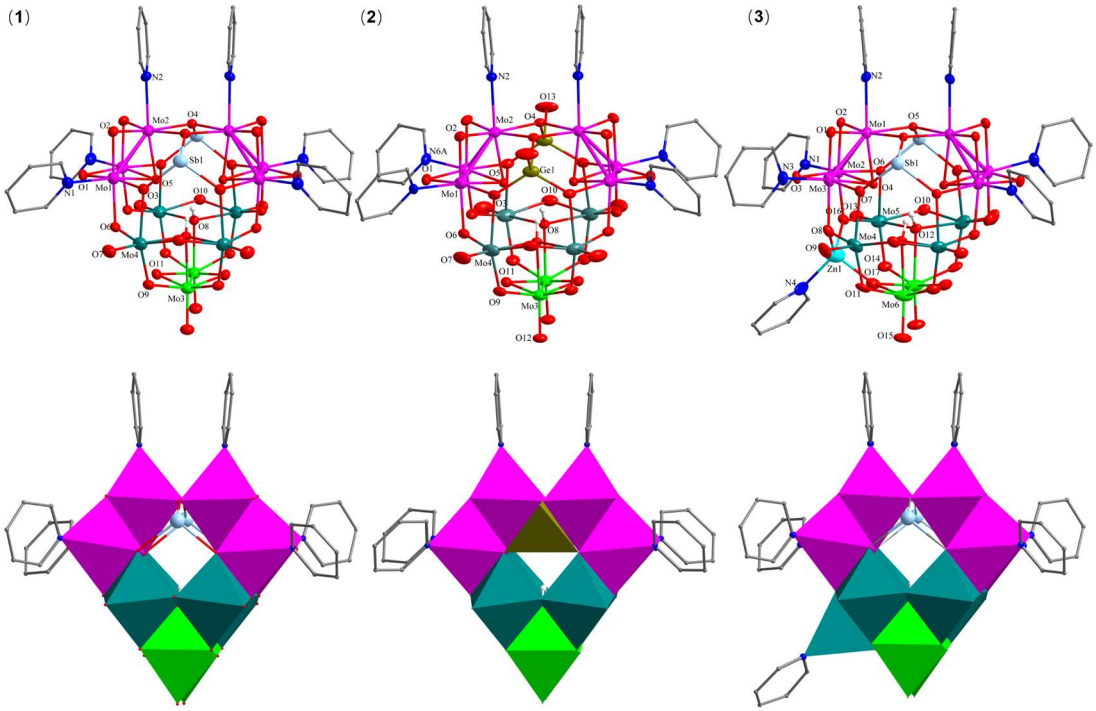

Figure S2. Atomically labeled structures and polyhedral presentation of **1-3** with 50% (30%) thermal ellipsoids for metal (O, N). Hydrogen atoms of pyridine are omitted for clarity.

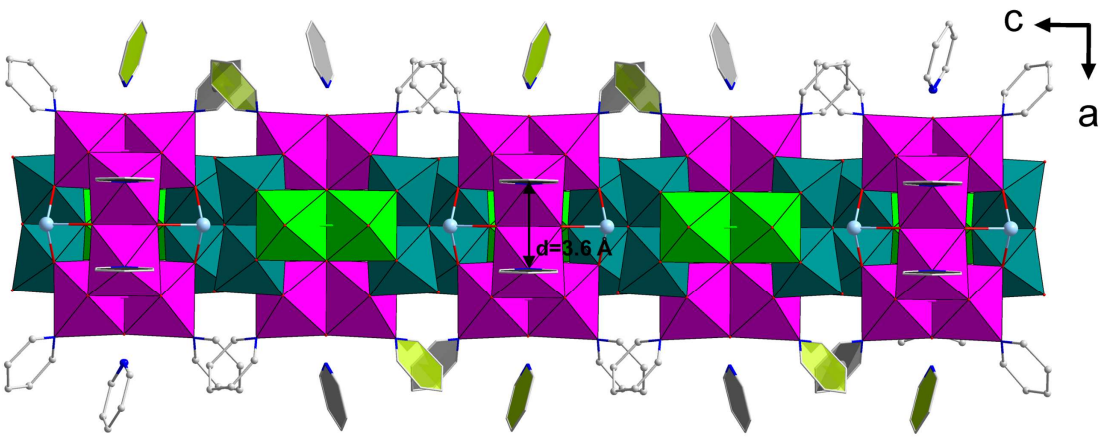

Figure S3. Crystal structure of the Mo^{IV}_6-Keggin anions **1**/**2** showing intra-(black six-membered ring) and intermolecular (gray and green six-membered ring) π···π packing interactions.

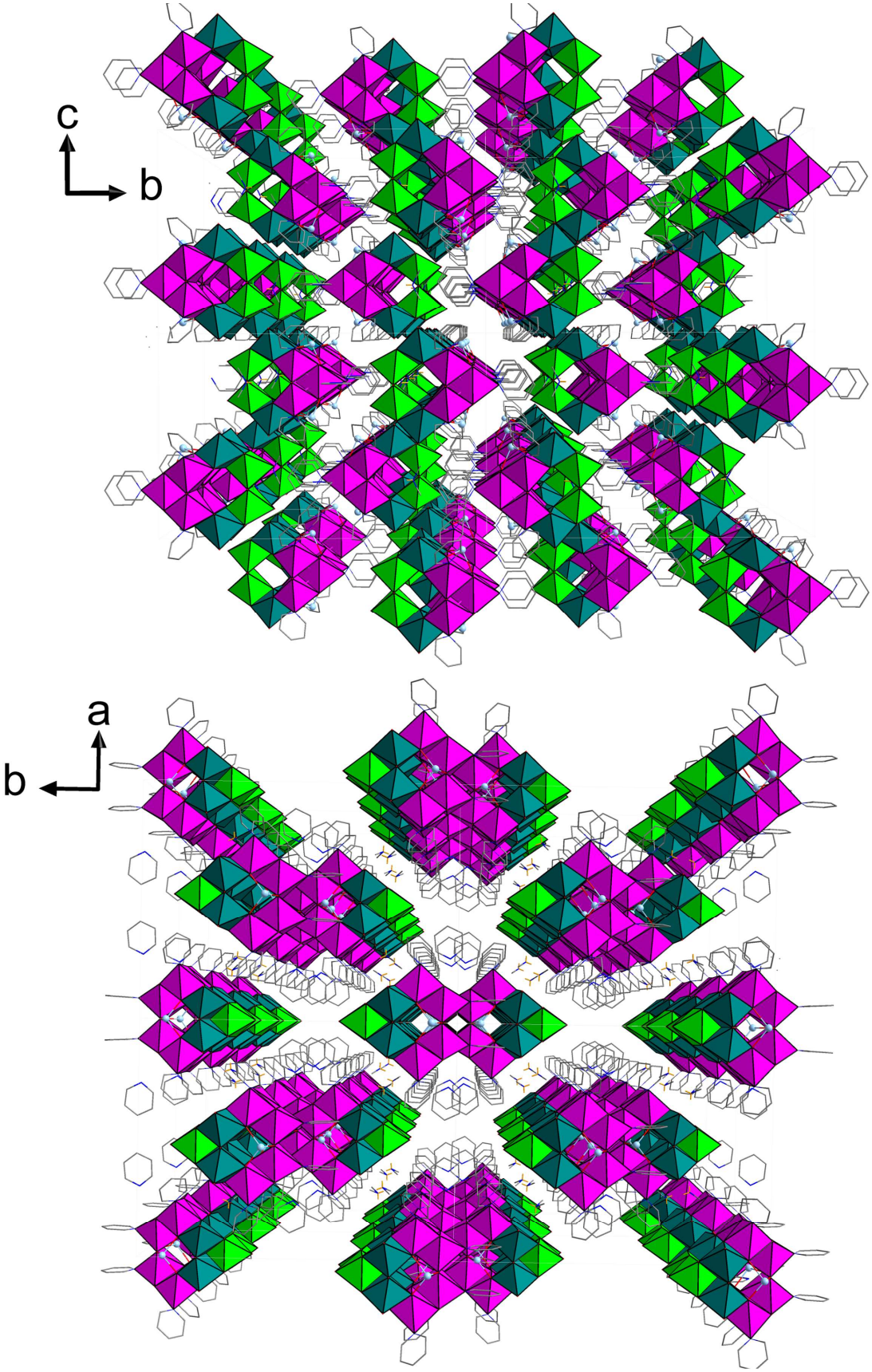

Figure S4. Crystal packing diagrams of Mo^{IV}_6-POM**1**. Polyhedral color code: Mo^{IV}, pink; Mo^{V}, green; Mo^{VI}, teal. Hydrogen atoms of pyridine molecules are omitted for clarity.

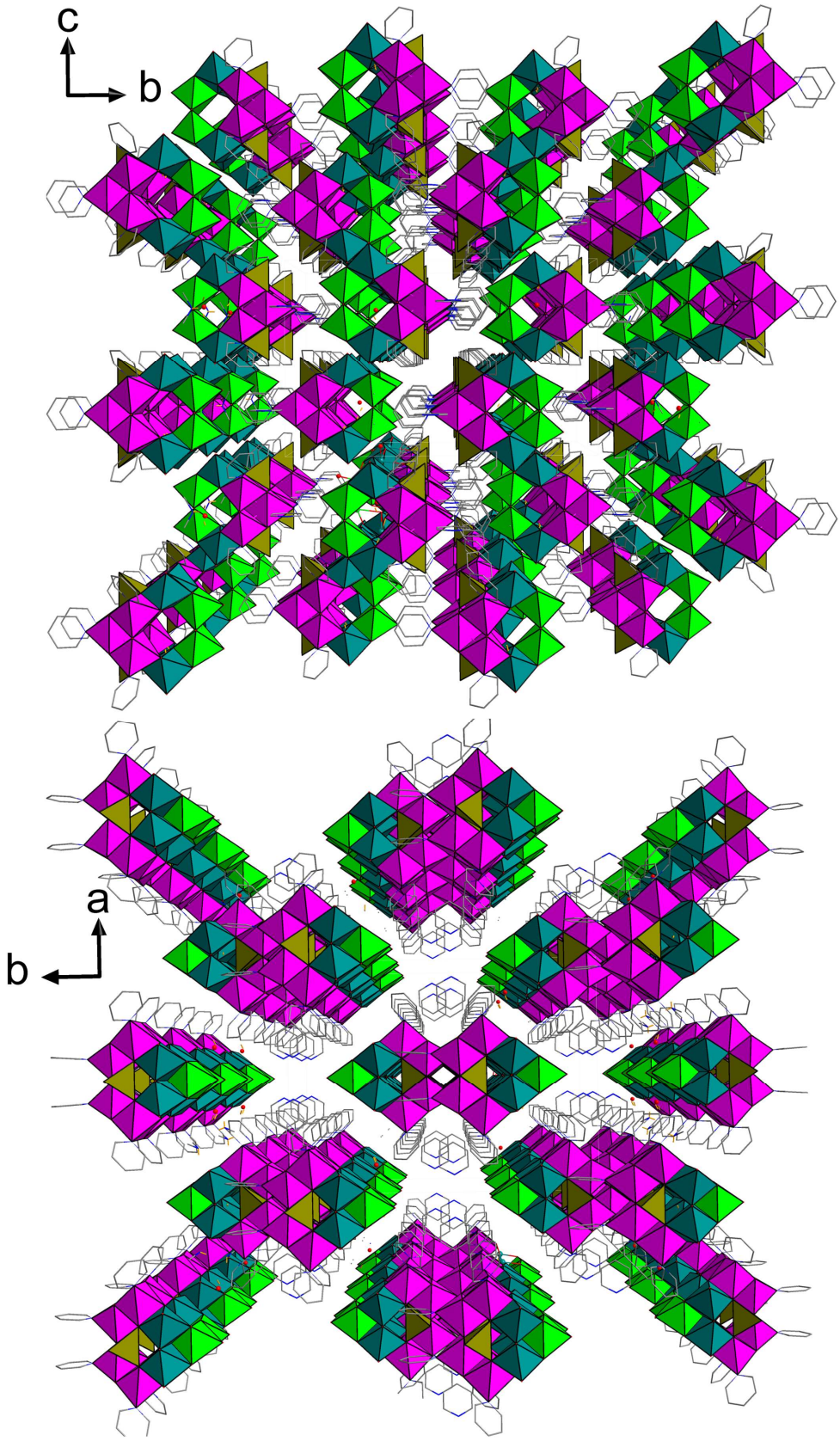

Figure S5. Crystal packing diagrams of Mo^{IV}_6-POM**2**. Polyhedral color code: Mo^{IV}, pink; Mo^{V}, green; Mo^{VI}, teal. Hydrogen atoms of pyridine molecules are omitted for clarity.

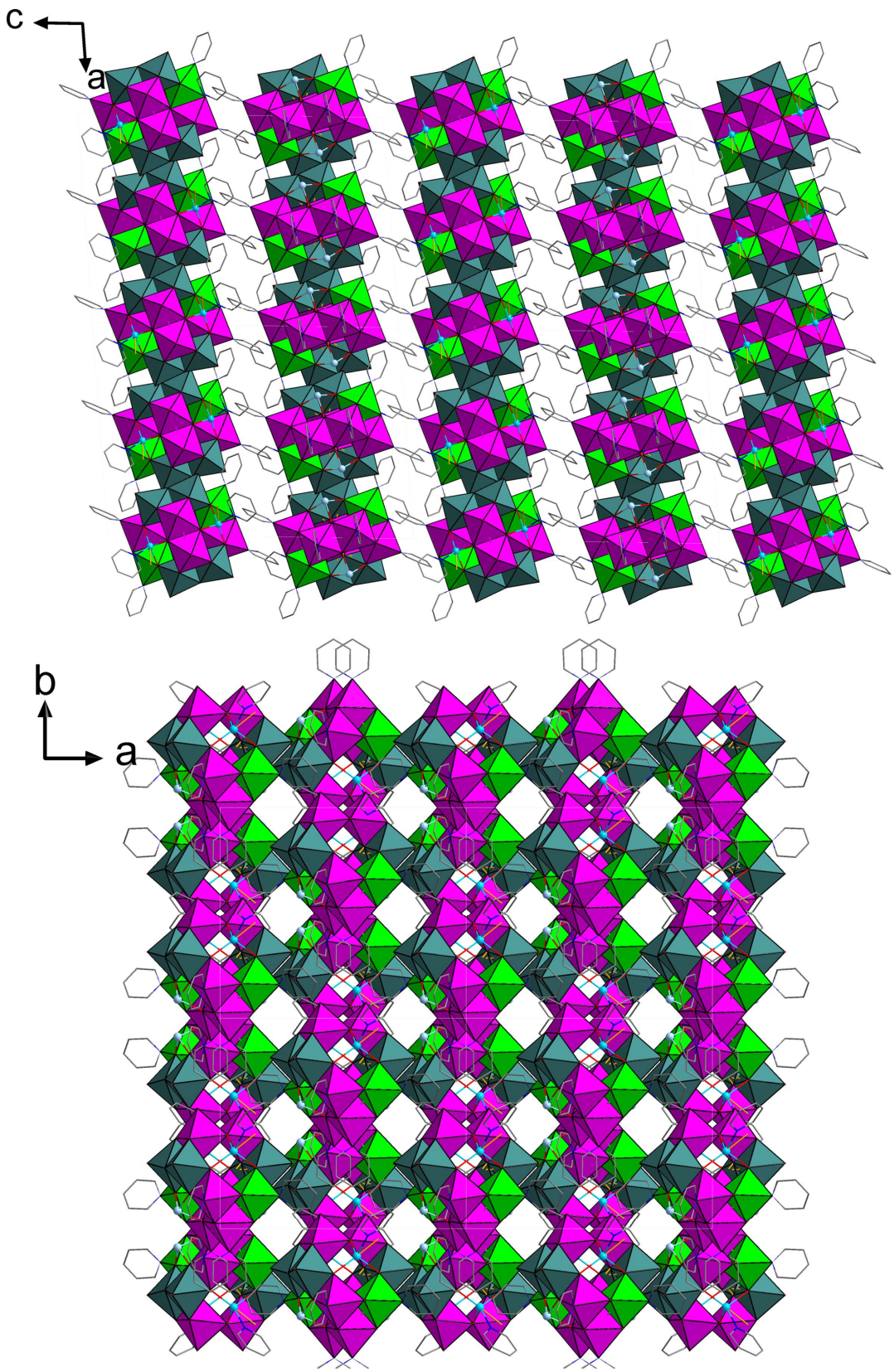

Figure S6. Crystal packing diagrams of Mo^{IV}_6-POM**3**. Polyhedral color code: Mo^{IV}, pink; Mo^{V}, green; Mo^{VI}, teal. Atom colour code: Zn, cyan; Sb, dark yellow. Hydrogen atoms of pyridine molecules are omitted for clarity.

Table S2. A comparison of bond lengths (Å) and LCF-dependent catalysis yields (%) of Mo^{IV}_3-POMs **1**-**28** and $[Mo^{IV}_3O_4(C_2O_4)_3Mepy_3]^{2-}$.

Electron-rich Mo^{IV}_3-POMs	Mo^{IV}_3	Mo^{V}_2	Mo^{IV}-O_b-Mo^{IV}	Mo^{IV}-O_b-M	LCF	Yield[b]	ref.
14*e*-$[Sb^{III}_2Mo^{IV}_6Mo^{V}_2Mo^{VI}_4O_{32}(OH)_2py_6]^{2-}$ (**1**)	2.505	2.595	1.935	1.991(Mo^{VI}) 2.128(Sb^{III})			This work
14*e*-$[(Ge^{IV}_2Mo^{IV}_6Mo^{V}_2Mo^{VI}_4O_{34}(OH)_2py_6]^{4-}$ (**2**)	2.496	2.589	1.928	1.988(Mo^{VI}) 2.145(Ge^{IV})			This work
14*e*-$[Sb^{III}_2Mo^{IV}_6Mo^{V}_2Mo^{VI}_4ZnO_{32}(OH)_2py_7]^{2-}$ (**3**)	2.500	2.613	1.921	2.031(Zn^{IV}) 2.115 (Sb^{III})			This work
12*e*-$[Mo^{IV}_3Mo^{V}_6Mo^{VI}_4O_{32}(OH)_2]$ (**4**)	2.503	2.592	1.982	2.033	-	17.5	[27]
12*e*-$[Mo^{IV}_3Mo^{V}_6Mo^{VI}_4O_{32}(OH)(OMe)]$ (**5**)	2.507	2.610	1.919	2.007	-	-	[27]
12*e*-$[Mo^{IV}_3Mo^{V}_6Mo^{VI}_4O_{32}(OH)(OEt)]$ (**6**)	2.494	2.585	1.933	2.096	-	-	[27]
12*e*-$[Mo^{IV}_3Mo^{V}_6Mo^{VI}_4O_{32}(OH)(OPr)]$ (**7**)	2.529	2.598	1.977	2.023	-	-	[27]
12*e*-$[Mo^{IV}_3Mo^{V}_6Mo^{VI}_4O_{32}(OH)(OCH_2H_4OH)]$ (**8**)	2.504	2.597	1.910	2.108	-	-	[27]
11*e*-$[Mo^{IV}_3Mo^{V}_5Cr^{III}Mo^{VI}_4O_{32}(OH)_2]$ (**9**)	2.513	2.586	1.919	2.102	-	12.1	[27]
12*e*-$[Mo^{IV}_3Mo^{V}_6Mo^{VI}W^{VI}_3O_{32}(OH)_2]$ (**10**)	2.482	2.594	2.024	2.037	-	-	[27]
12*e*-$[Mo^{IV}_3Mo^{V}_6W^{VI}_4O_{33}(OH)]^{-}$ (**11**)	2.508	2.597	1.906	2.087	-	-	[27]
6*e*-*α*-$[Mo^{IV}_3Mo^{VI}W_8O_{30}(OH)_7py_3]^{2-}$ (**12**)	2.503	-	1.917	2.050	-	-	[21]
12*e*-*γ*-$[Mo^{IV}_6Mo^{VI}_6O_{28}(OH)_6py_6]^{3-}$ (**13**)	2.523	-	1.942	2.044	-	13.3	[21]
12*e*-*γ*-$[Mo^{IV}_6W^{VI}_6O_{29}(OH)_5py_6]^{3-}$ (**14**)	2.518	-	1.936	2.092	-	12.3	[21]
12*e*-*γ*-$[Mo^{IV}_6W_6{}^{VI}O_{29}(OH)_5Na(H_2O)_5py_6]^{2-}$ (**15**)	2.512	-	1.924	2.060	Mo^{IV}_3•••$O_3W^{VI}_2$	42.7	[21]
12*e*-*γ*-$[Mo^{IV}_6Mo^{VI}_7O_{36}py_6]^{4-}$ (**16**)	2.511	-	1.926	2.087	Mo^{IV}_3•••$O_5Mo^{VI}_3$	100	[23]
12*e*-*β*-$[Mo^{IV}_6Mo^{VI}_7O_{36}py_6]^{4-}$ (**17**)	2.525	-	1.939	2.090	-	78	[7,23]
18*e*-$[Mo^{IV}_6Mo^{V}_6Mo^{VI}_9O_{58}]^{8-}$ (**18**)	2.501	2.710	1.914	2.141	-	16.9	[20]
36*e*-$[Al_2Mo^{IV}_{12}Mo^{V}_{12}Mo^{VI}_6O_{77}(OH)_2(H_2O)py_{12}]^{6-}$(**19**)	2.510	2.671	1.930	2.103[a]	-	66	[22]
36*e*-$[V_2Mo^{IV}_{12}Mo^{V}_{12}Mo^{VI}_6O_{81}(OH)_2(H_2O)py_{12}]^{12-}$(**20**)	2.490	2.846	1.946	2.138[a]	Mo^{IV}_3•••$\{O_8Mo^{VI}_4\}_3$	100	[22]
36*e*-$[Mo_2Mo^{IV}_{12}Mo^{V}_{12}Mo^{VI}_6O_{81}(OH)_2(H_2O)py_{12}]^{8}$(**21**)	2.490	2.852	1.931	2.125[a]	Mo^{IV}_3•••$\{O_8Mo^{VI}_4\}_3$	100	[22]
28*e*-$[NaMo^{IV}_{12}Mo^{V}_4Mo^{VI}_3O_{44}py_{12}]^{-}$ (**22**)	2.512	2.674	1.932	2.011	-	40.8	[10]
6*e*-$[ZnMo^{IV}_3Mo^{VI}_{10}P_4O_{49}py_3]^{4-}$ (**23**)	2.545	-	1.936	2.088	-	47.9	[10]
6*e*-$[Sb_3Mo^{IV}_3Mo^{VI}_{15}O_{57}py_3]^{3-}$ (**24**)	2.527	-	1.927	2.055	Mo^{IV}_3•••$Sb^{III}O_4$	100	[24]
12*e*-$[Ge_3Mo^{IV}_6Mo^{VI}_{10}O_{48}py_6]$ (**25**)	2.487	-	1.930	2.086[a]	-	46.9	[20]
12*e*-$[ZnGe_2Mo^{IV}_6Mo^{VI}_{10}O_{48}py_6]$ (**26**)	2.497	-	1.921	2.019	-	-	[20]
12*e*-1D-$[Mo^{IV}_6Mo^{VI}_4Ge_2ZnO_{31}]^{4-}$ (**27**)	2.510	-	1.930	2.089	-	-	[26]
6*e*-2D-$[Mo^{IV}_3Mo^{VI}_9Zn_6P_7O_{56}]^{+}$ (**28**)	2.536	-	1.970	2.042	-	-	[26]
$[Mo^{IV}_3O_4(C_2O_4)_3Mepy_3]^{2-}$	2.499		1.918		-	3.9	5

[a] μ_3-O linking Mo^{IV}_3 and neighboring metal atoms. [b] $PhNO_2 \rightarrow PhNH_2$ (NH_2NH_2, 80°C, 2 hours, EtOH, 3% catalyst)

S-7 Band valance sum (BVS) calculations of 1-3

Table S3. BVS results for **1**.

[**1**]			
Sb1 3.107	O1 1.938	O6 2.315	O11 2.041
Mo1 4.271	O2 2.006	O7 1.994	O12 1.990
Mo2 4.093	O3 2.158	**O8 1.046**	
Mo3 5.126	O4 2.345	O9 2.051	
Mo4 5.952	O5 2.012	O10 1.811	

Table S4. BVS results for **2**.

[**2**]			
Ge1 3.930	O1 2.022	O6 2.328	O11 2.071
Mo1 4.290	O2 2.148	O7 1.865	O12 2.115
Mo2 4.150	O3 2.077	**O8 1.005**	**O13 0.877**
Mo3 5.188	O4 1.956	O9 2.067	
Mo4 6.026	O5 2.385	O10 1.855	

Table S5. BVS results for **3**.

[**3**]			
Sb1 2.950	Mo6 5.235	O7 2.139	O14 2.022
Zn1 1.563	O1 2.129	**O8 0.916**	O15 2.228
Mo1 4.213	O2 2.165	O9 1.899	O16 1.977
Mo2 4.282	O3 1.998	O10 2.102	O17 2.058
Mo3 4.194	O4 2.385	O11 2.201	
Mo4 5.959	O5 2.132	O12 1.948	
Mo5 6.005	O6 2.206	O13 2.082	

S-8 Spectroscopic characterization

S8-1 TGA

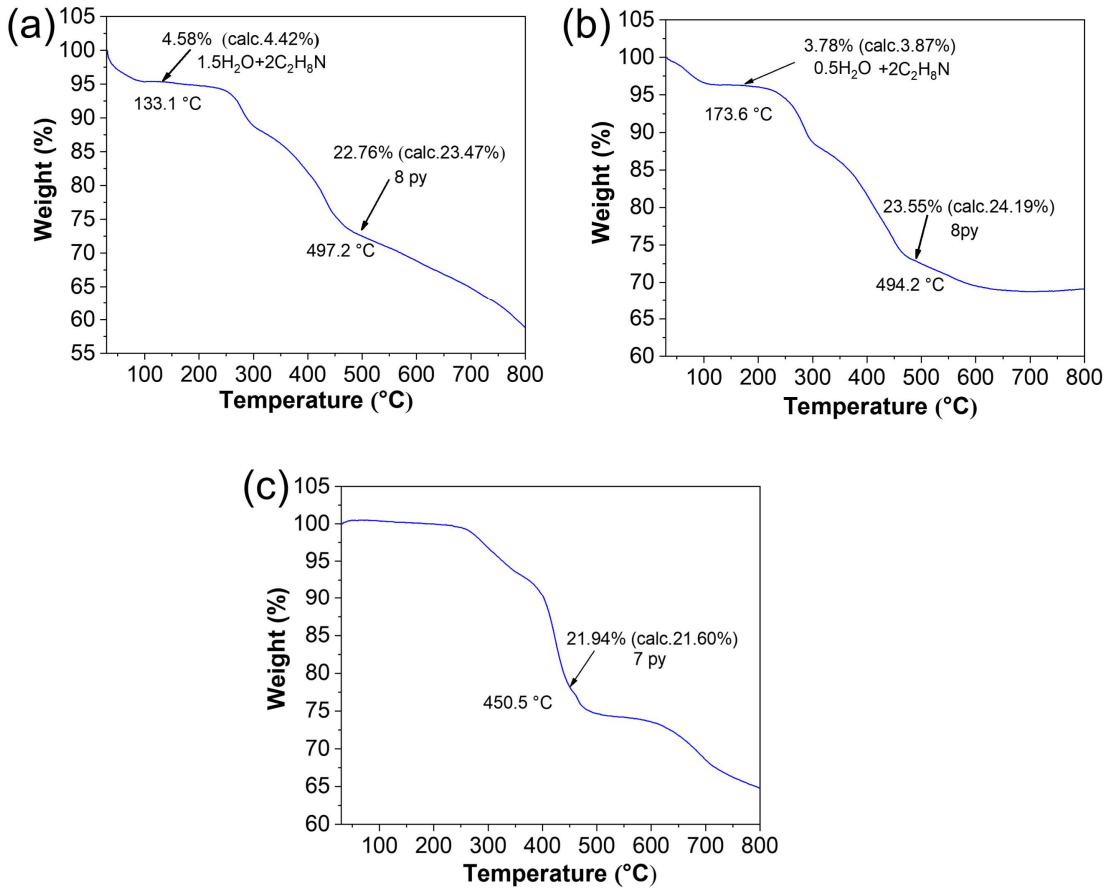

Figure S7. Thermogravimetric analysis (TGA) of Mo^{IV}_6-POMs**1**-**3** sample (a-c) from 30-800 °C under Nitrogen atmosphere.

For Mo^{IV}_6-POM**1**, the weight loss in the temperature range of 30-133 °C correspond to the loss of 1.5 lattice water and 2 solvent dimethylamine (C_2H_8N), and the weight loss between 133-500 °C is associated with the loss of 8 pyridine. For Mo^{IV}_6-POM**2**, the weight loss in the temperature range of 30-174 °C correspond to the loss of 0.5 crystal water and 2 solvent dimethylamine (C_2H_8N), the weight loss between 174-500 °C is associated with the loss of 8 pyridine. For Mo^{IV}_6-POM**3**, the weight loss in the temperature range of 200-450 °C correspond to the loss of 7 pyridine.

S8-2 XRD

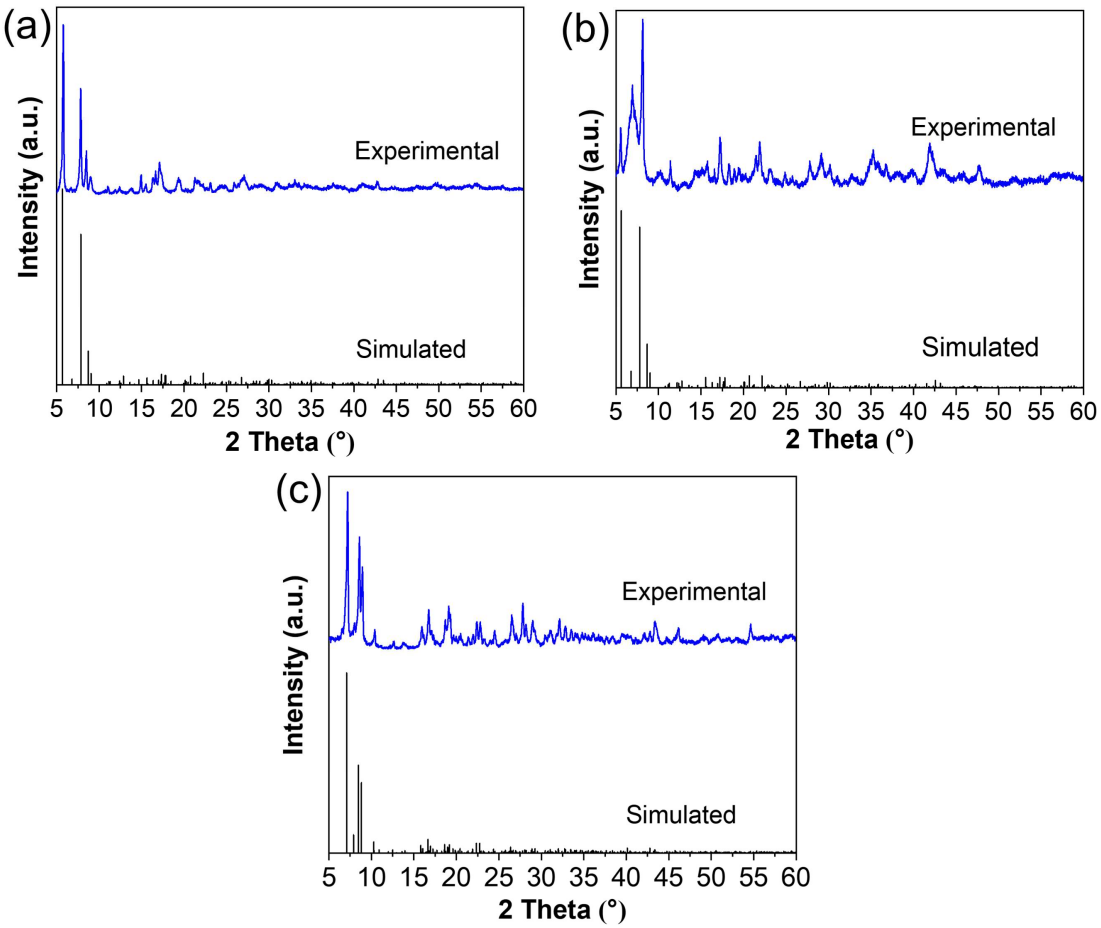

Figure S8. The powder XRD (blue line, PXRD) patterns and simulated PXRD (black line) pattern of Mo^{IV}_6-POMs**1**-**3** (a-c).

The intensity divergence of Mo^{IV}_6-POM**2** is owing to the different orientations of the powder sample during measurements.

S8-3 XPS

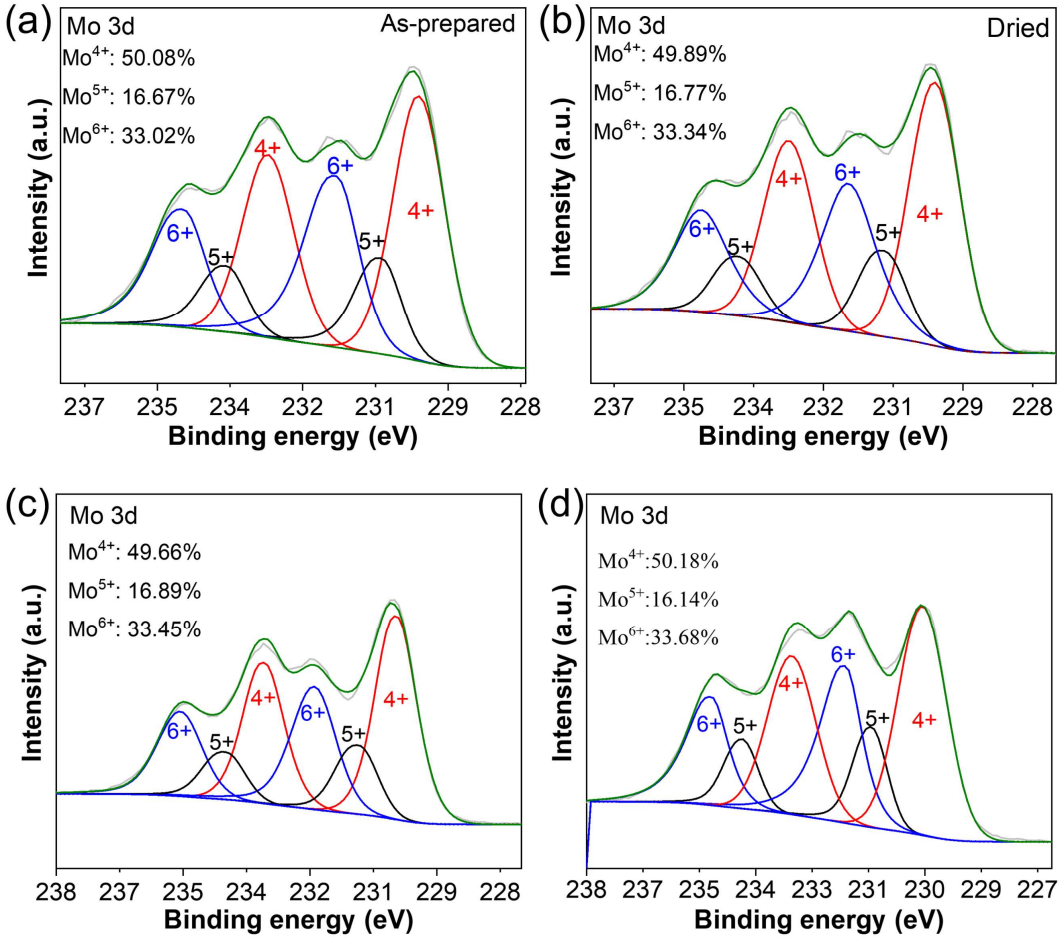

Figure S9. The high-resolution XPS spectra of as-prepared (a) and dried (b) of Mo^{IV}_6-POM**1** samle. The high-resolution XPS spectra of as-prepared Mo^{IV}_6-POMs**2**-**3** (c-d) in the Mo 3d region.

The high-resolution XPS of Mo 3d in Mo^{IV}_6-POM**1** could be fitted to six peaks at 235.1, 234.0, 233.1,231.9, 230.9 and 230.0 eV, which correspond to the binding energies of Mo(VI)-3d3/2, Mo(V)-3d3/2, Mo(IV)-3d3/2, Mo(VI)-3d5/2, Mo(V)-3d5/2, and Mo(IV)-3d5/2, respectively, thus exhibiting that the different valence states of Mo atoms in Mo^{IV}_6-POM**1** are IV and V and VI and the ratio of Mo^{IV}: Mo^{V}: Mo^{VI} is close to 6: 2: 4 and are in good agreement with single crystal diffraction results and the bond valence sum (BVS) calculation results (**Table S4**). The XPS spectra of as-prepared (Figure S9a) and dried (Figure S9b) samples of Mo^{IV}_6-POM**1** almost no changes, it also exhibits the Mo^{IV} are not be oxidized after the dried treatment and good thermal stability. The high-resolution XPS spectra of Mo^{IV}_6-POM**2** (Figure S9c) and Mo^{IV}_6-POM**3** (Figure S9d) are similar with that of Mo^{IV}_6-POM**1**.

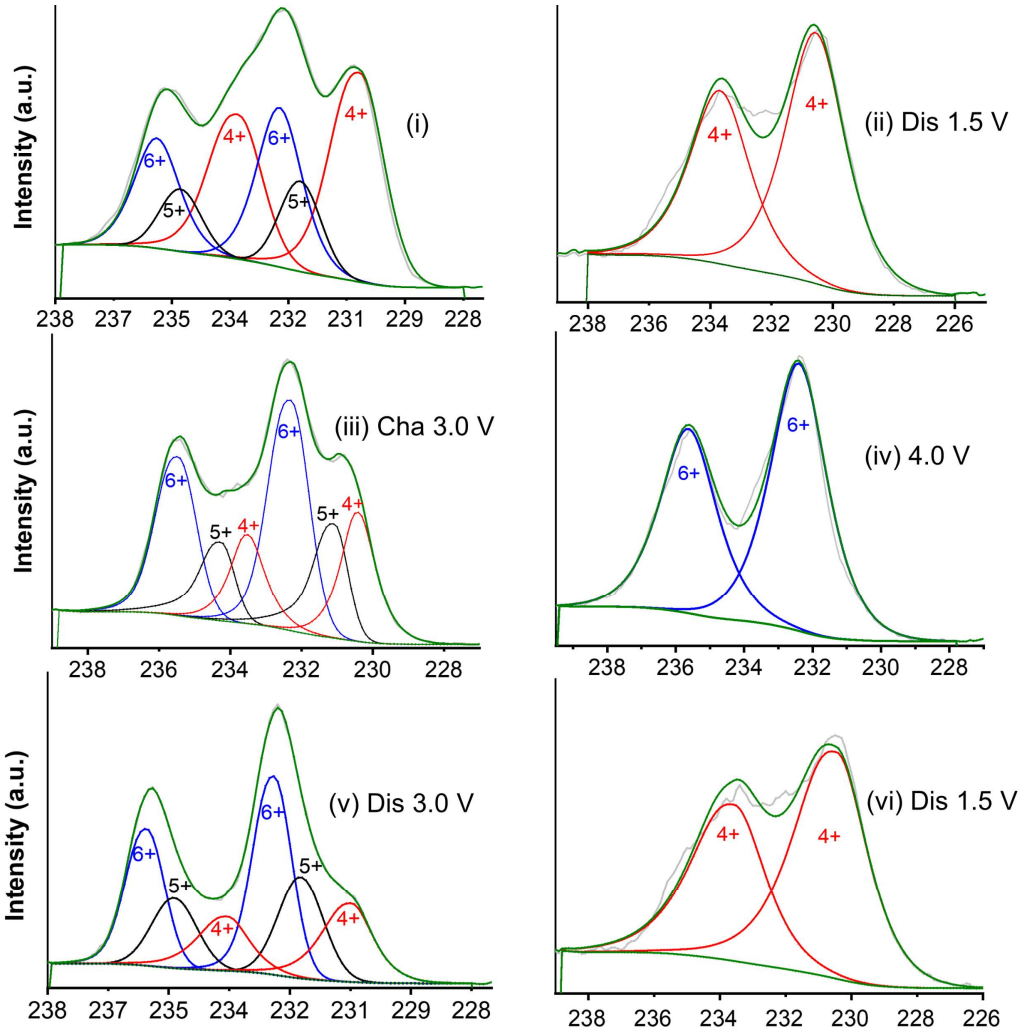

Figure S10. The high-resolution XPS spectra of as-prepared Mo^{IV}_6-POM**1** in the Mo 3d region at different cutoff voltages.

Table S6. The relevant parameters for XPS spectras fitting.

	Binding Energy (eV)					
	Mo(IV)-3d5/2	Mo(IV)-3d3/2	Mo(V)-3d5/2	Mo(V)-3d3/2	Mo(VI)-3d5/2	Mo(VI)-3d3/2
i pristine	229.64	232.76	231.06	234.15	231.75	234.92
ii dis 1.5	230.46	233.57	-	-	-	-
iii cha 3.0	230.27	233.41	231.55	234.69	232.21	235.38
iv cha 4.0	-	-	-	-	232.40	235.63
v dis 3.0	230.47	233.54	231.73	234.87	232.40	235.55
vi dis 1.5	230.56	233.69	-	-	-	-

S8-4 FT-IR

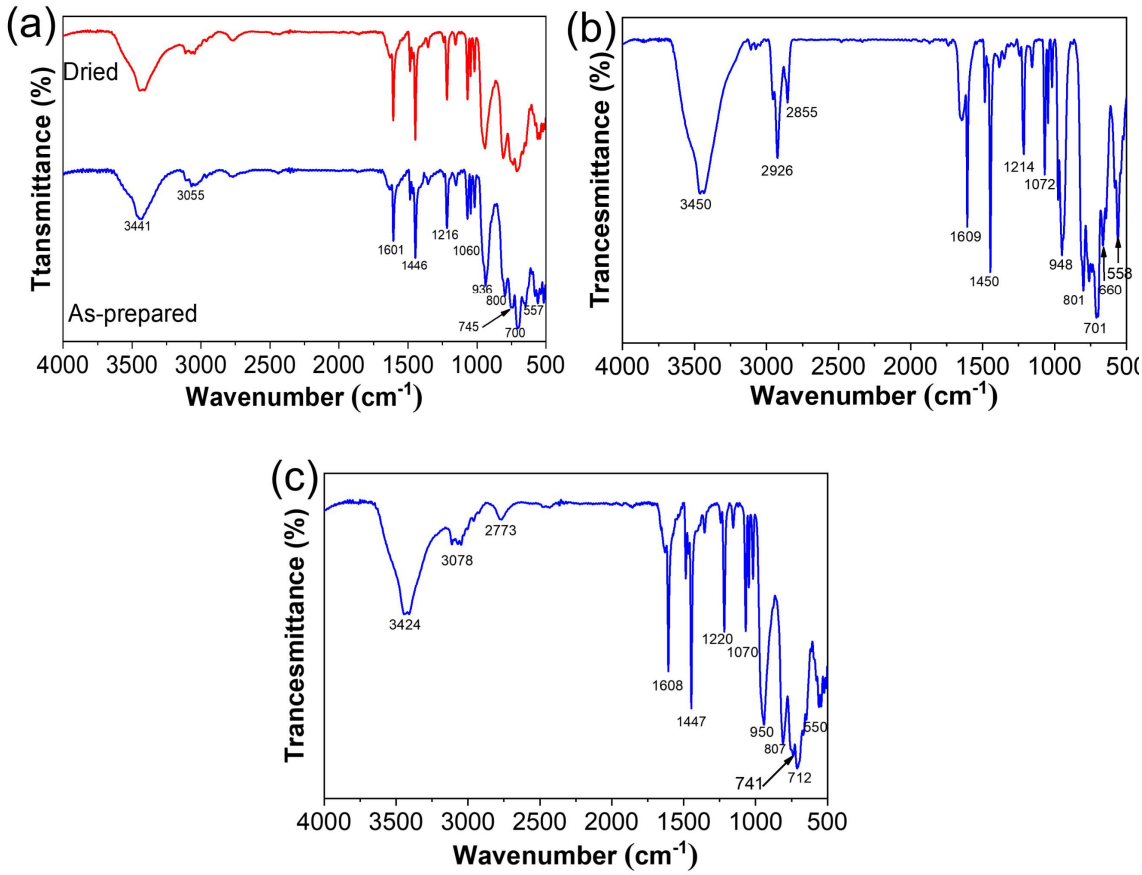

Figure S11. FT-IR spectra of dried (red line) and as-synthesized (blue line) Mo^{IV}_6-POM **1-3** (a-c). The Mo^{IV}_6-POMs**1** sample was dried at 110 °C for 10 hours.

The broad peaks at about 3424-3450 cm^{-1} can be classified as the N-H (dimethylamine) and O-H (H_2O) stretching vibration, the bands at 1601-1610 cm^{-1} are assigned to the in-plane bending vibration of the O-H and N-H groups (dimethylamine). The bands in 2826-2978 cm^{-1} and around 1450 cm^{-1} attributed to C-H stretching (pyridine and dimethylamine). The bands in the region 1060-1072 and 1214-1220 cm^{-1} are belonging to stretching vibrations of C-N and C-C (pyridine and dimethylamine). The peak at 936-950 cm^{-1} is assigned to the stretching vibrations of the Mo-O_t groups. The peaks at around 801, 751 and 700 cm^{-1} regions can be attributed to the stretching of Mo-O-Mo groups. The band at around 660 and 557 cm^{-1} can be assigned to the (Mo-O-Mo) remaining stretching vibrations. The FT-IR spectra of dried Mo^{IV}_6-POM**1** is virtually unchanged from the original pattern of as-prepared one, and exhibits the molecular structure keep stable without damage after dried treatment.

S8-5 UV-vis

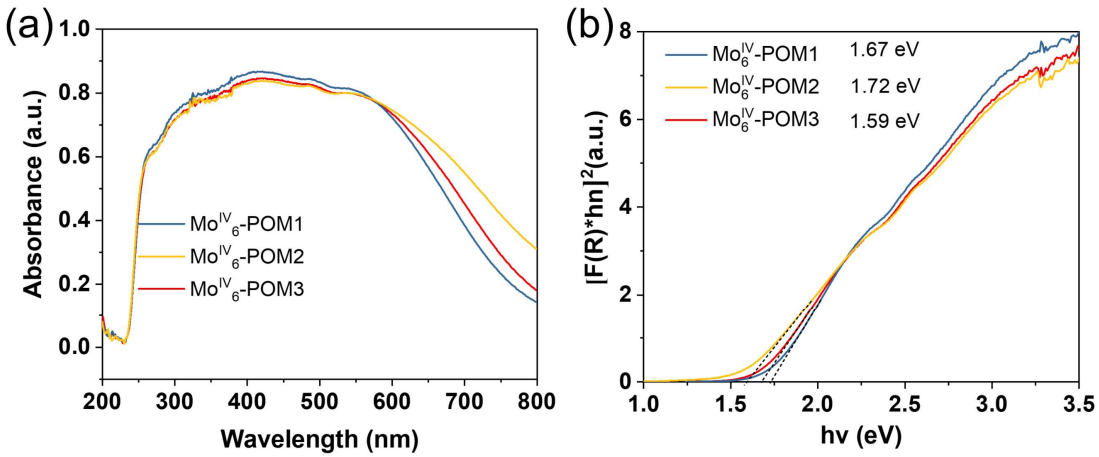

Figure S12. (a) The solid-state UV-vis spectra of Mo$^{IV}_6$-POMs**1**-**3**. (b) their transformation based on Tauc plot function. The inset indicates the calculated optical band gaps of four samples.

S-9 Electrochemical performance

Table S7. Electronic conductivity values of Mo^{IV}_6-POMs.

Sample	Electric conductivity (S cm^{-1})	Electric conductivity (S cm^{-1})		
		Sample 1	Sample 2	Sample 3
Mo^{IV}_6-POM**1**	4.61×10^{-9}	4.93×10^{-9}	4.35×10^{-9}	4.56×10^{-9}
Mo^{IV}_6-POM**2**	2.72×10^{-9}	2.69×10^{-9}	2.94×10^{-9}	2.53×10^{-9}
Mo^{IV}_6-POM**3**	2.91×10^{-10}	2.71×10^{-10}	2.84×10^{-10}	3.17×10^{-10}

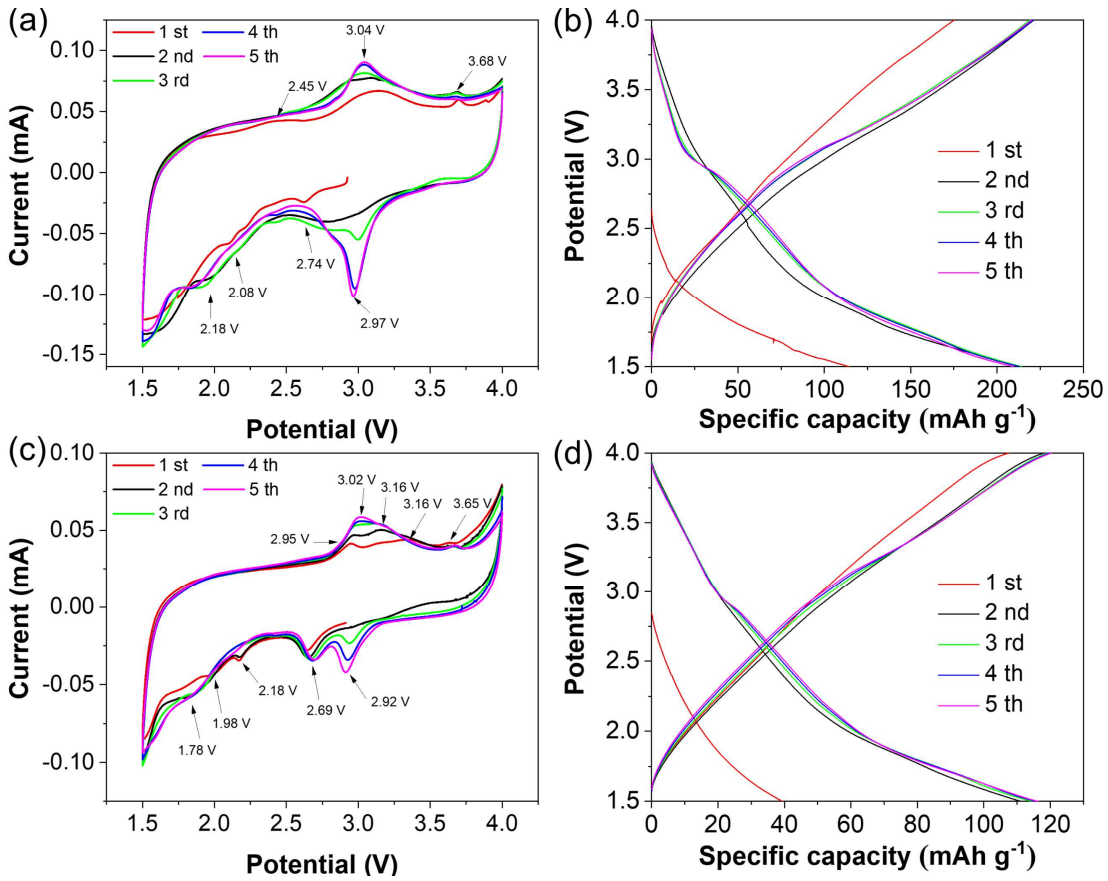

Figure S13. CV curves at a scan rate of 0.5 mV s^{-1} and galvanostatic charge/discharge voltage profiles (1.0 A g^{-1}) of 1 st to 5 th cycles for Mo^{IV}_6-POM **2** (a, b) and Mo^{IV}_6-POM **3** (c, d) over the voltage range of 1.5-4.0 V (vs. Li/Li^+).

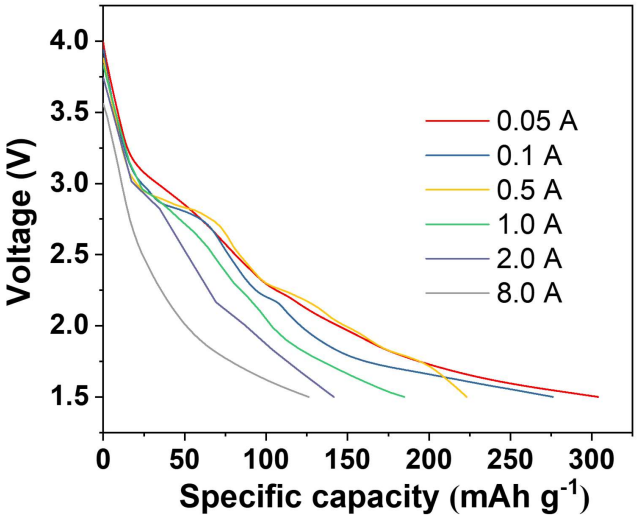

Figure S14. Discharge curves for Mo^{IV}_6-POM **1** over the voltage range of 1.5-4.0 V (vs. Li/Li^+) at various current density.

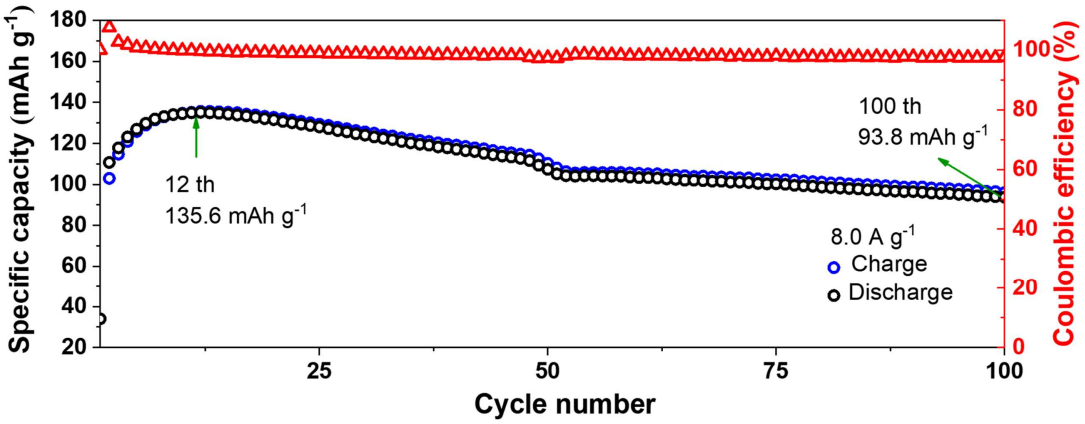

Figure S15. Cycling performance with coulombic efficiency of Mo^{IV}_6-POM**2** at the current density of 8.0 A g^{-1} for 100 cycles.

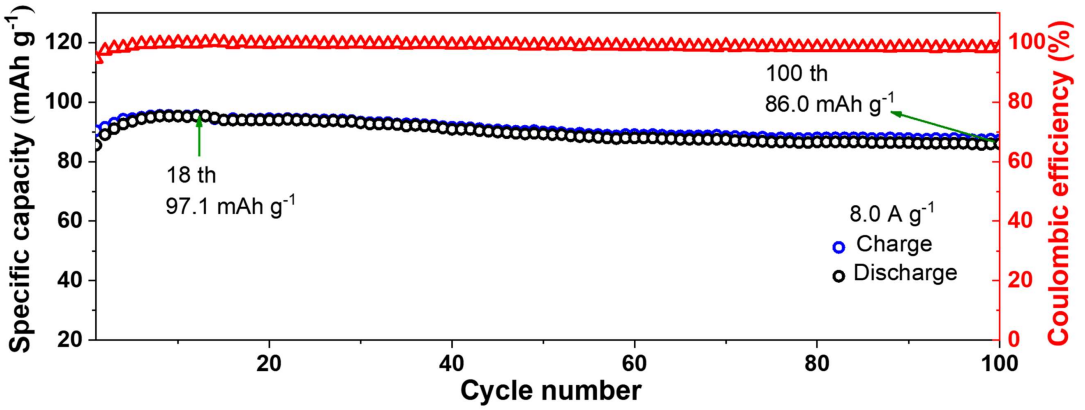

Figure S16. Cycling performance with coulombic efficiency of Mo^{IV}_6-POM**3** at the current density of 8.0 A g^{-1} for 100 cycles.

Table S8. Comparison of electrochemical performance of reported POM-type cathode materials.

Cathode	Active materials ratio (%)	RSC (mA h g^{-1})/ RC (mA g^{-1})	Potential range (V)	Refs
NAM hand KB	32%	134/180 (0.4 C) (30 cycles)	1.5-4.0	[53]
SiW_{12}/rGO	20%	120/2000 (10 cycles)	1.5-4.2	[22]
SiW_{12}	10%	150/50 (20 cycles)	1.5-4.2	[22]
Mn12	10%	~75/ 0.01 mA cm^2 (10 cycles)	2.0-4.0	[6]
SWNT–POM nano hybrids	10%	300/1 mA (10 cycles)	1.5-4.2	[19]
PMo12-MCBs	30%	50/1.0 mA (10 cycles)	1.5-4.2	[7]
$TBA_3[PMo_{12}O_{40}]$	10%	260/1 mA (10 cycles)	1.5-4.2	[14]
$TBA_3[PMo_{12}O_{40}]$/S-rGO	10%	300/1 mA (100 cycles)	1.5-4.2	[24]
$TBA_3[PMo_{12}O_{40}]$/SWNT	10%	300/ 1 mA (10 cycles)	1.5-4.2	[20]
PMo12/RGO	10%	135/1 mA (10 cycles)	1.5-4.2	[17]
$K_3[PMo_{12}O_{40}]$	30%	100/50 μA (10 cycles)	1.5-4.2	[18]
$K_{5.72}H_{3.28}[PV_{14}O_{42}]$ (KPV)	30%	140/100 μA (50 cycles)	1.5-4.2	[8]
PANI/PMo_{12}	~57%	149.5/27(0.1 C) (50 cycles)	1.5-4.2	[21]
PW_{12}	50%	40/200 (50 cycles)	1.5-4.2	[23]
PANI/PW_{12}	~57%	110/200 (50 cycles)	1.5-4.2	[23]
rGO@PANI/PW_{12}	-	80/2000 (1000 cycles)	1.5-4.2	[23]
Mo^{IV}_6-POM**1**	30%	122/8000 (100 cycles)	1.5-4.0	This work
Mo^{IV}_6-POM**2**	30%	143/2000 (100 cycles)	1.5-4.0	This work
Mo^{IV}_6-POM**3**	30%	117/2000 (100 cycles)	1.5-4.0	This work

RSC: Reversible specfic capacity. CR: Charge rate.

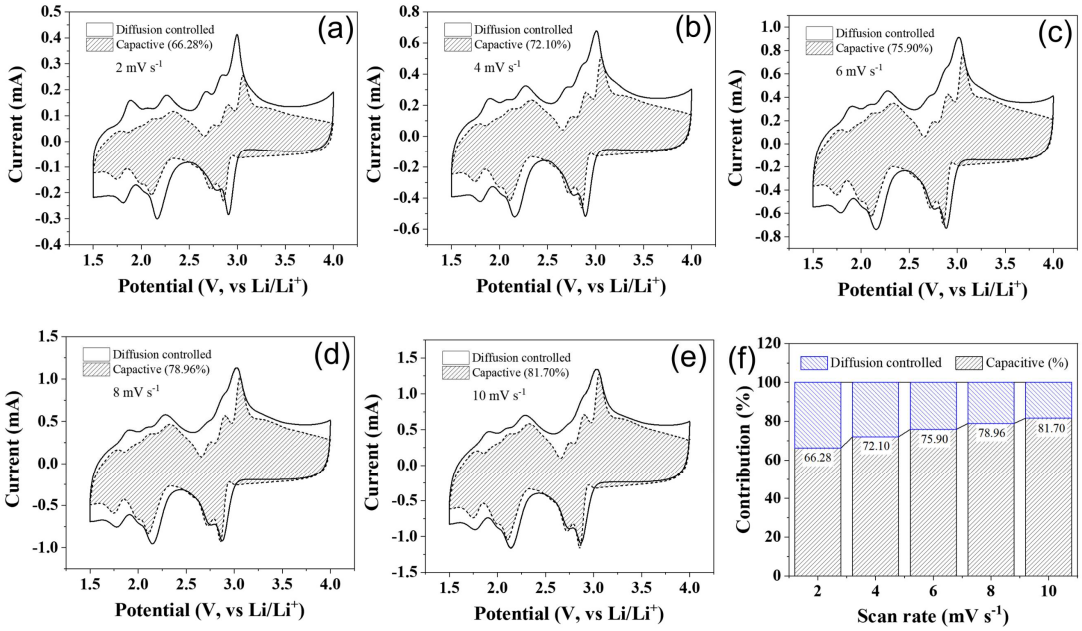

Figure S17. Percentages of capacitive and diffusion-controlled capacities at different scan rates (2-10 mV s^{-1}) of Mo^{IV}_6-POM**1**.

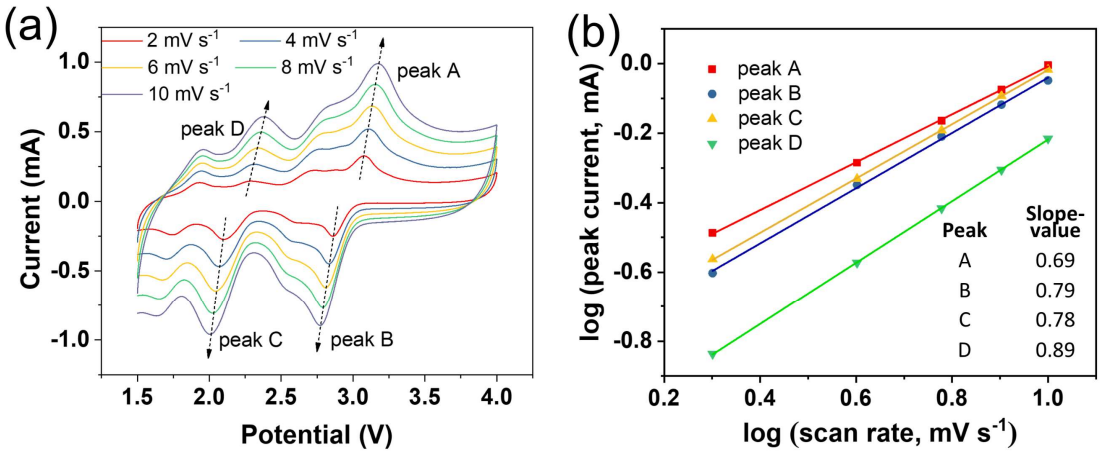

Figure S18. (a) Rate-scan CV curves of the Mo^{IV}_6-POM**2** at various sweep rates. (b) Peak current I_p as a function of square root of scan rate $v^{0.5}$.

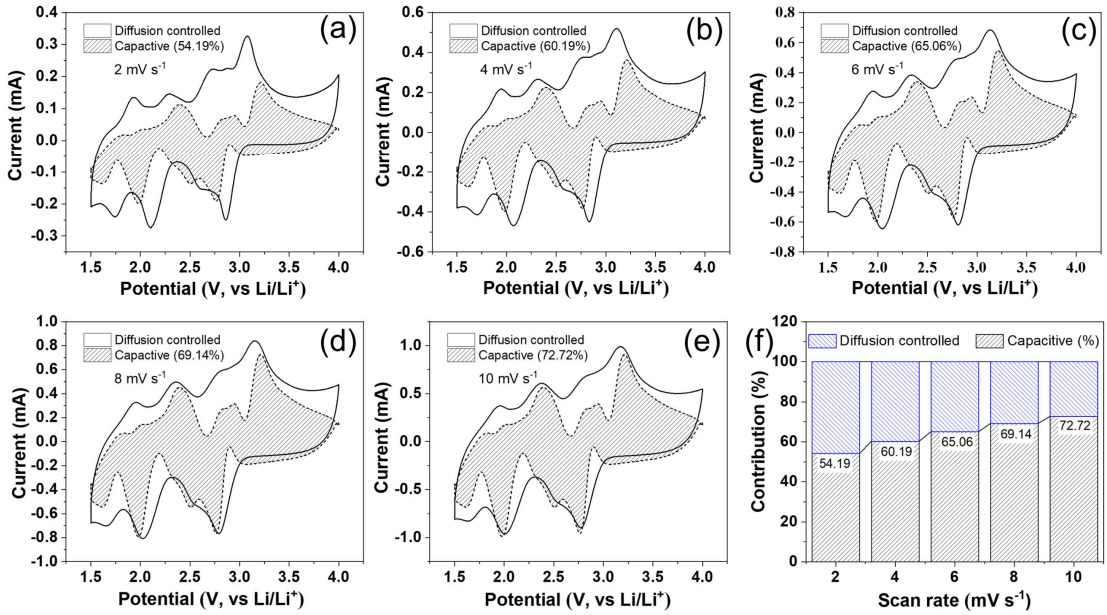

Figure S19. Percentages of capacitive and diffusion-controlled capacities at different scan rates (2-10 mV s^{-1}) of Mo^{IV}_6-POM **2**.

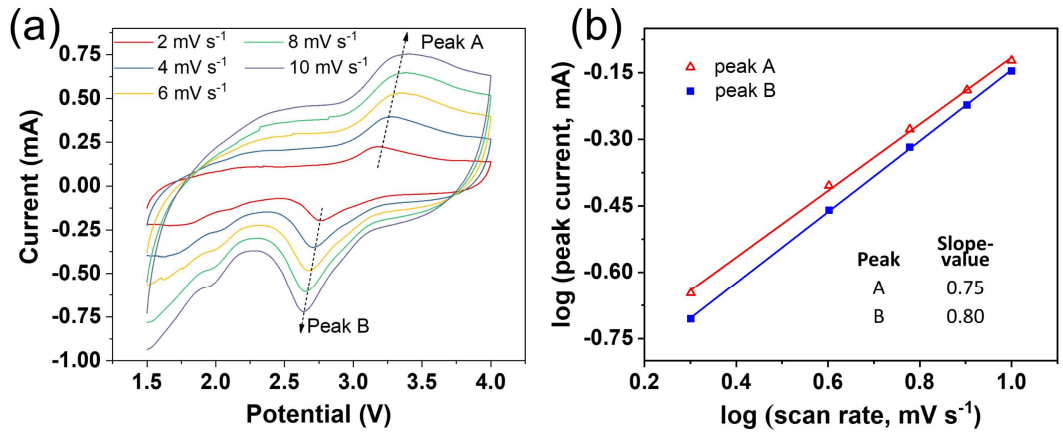

Figure S20. (a) Rate-scan CV curves of the Mo^{IV}_6-POM**3** at various sweep rates. (b) Peak current Ip as a function of square root of scan rate $v^{0.5}$.

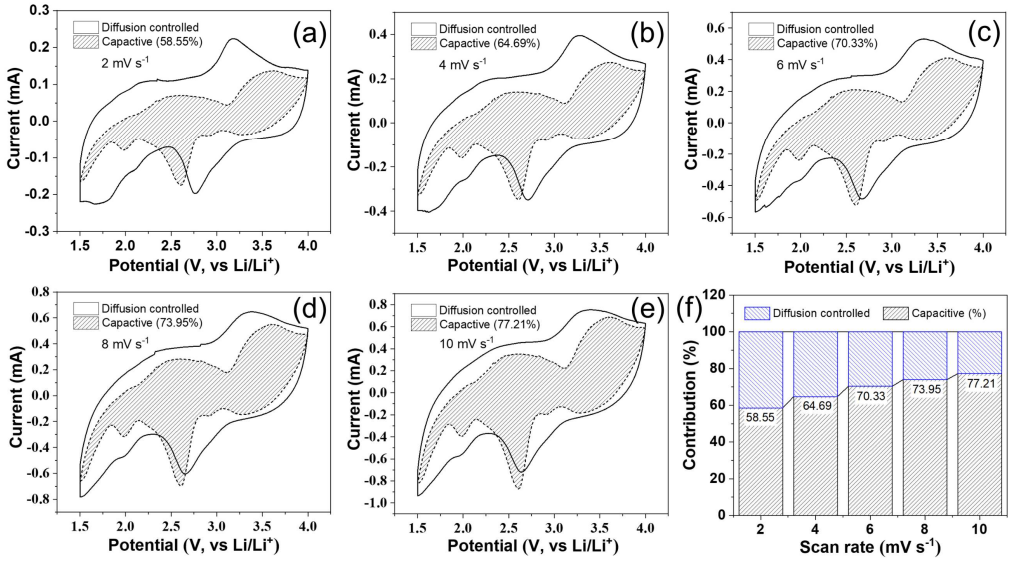

Figure S21. Percentages of capacitive and diffusion-controlled capacities at different scan rates (2-10 mV s^{-1}) of Mo^{IV}_6-POM**3**.

S-10 DFT calculations

All the density functional theory (DFT)[9] calculations were performed using Gaussian 09. D01 program[10] at the B3LYP[11]/lanl2DZ[12] level of theory. The single point calculation was performed using B3LYP functional with the 6-31G* basis sets for main-group atom (C, H, O and N) and the pseudopotential basis sets LANL2DZ[12] for the metal atoms (Mo, Ge, Sb and Zn). In all the calculations, a closed-shell singlet state was assumed and spin-restricted MOs was used.

S10-1 Model structure of 24e-1

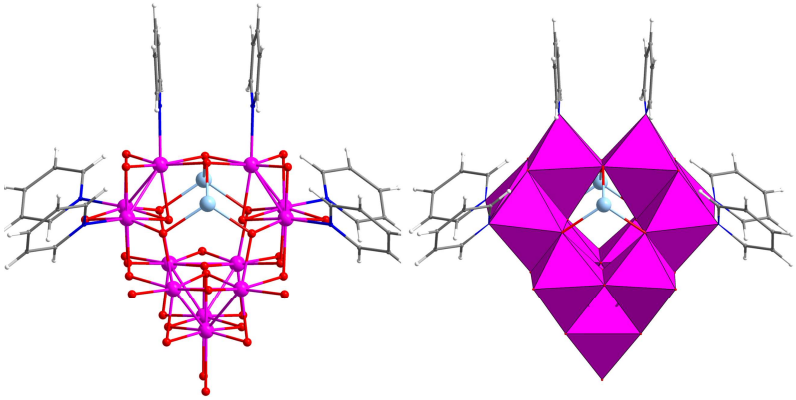

Figure S22. Polyhedral and ball-and-stick representation presentation of super reduced-state structure of Mo^{IV}_6-POM**1** (24e-**1**). Color code same as Figure 1a.

Wang and coworkers[4b] construct Keggin super reduced structure $[PMo^{IV}_{12}O_{40}]^{27-}$ from original Keggin $[PMo^{VI}_{12}O_{40}]^{3-}$ structure though assembling four $[Mo_3^{IV}O_4]$ building blocks. The distance of Mo-O_b, Mo^{VI}_3-μ_3-O and Mo-Mo were determined as 1.92-1.96, 2.02-2.04 and 2.5-2.6 Å, respectively, and hence construct the $[Mo_3^{IV}O_4]$ building block, based on In Operando Extended X-ray absorption fine structure (EXAFS) analyses and related paper.

The *ex-situ* XPS and FT-IR measurements exhibit that all of four Mo^{6+} and two Mo^{5+} atoms of **1** were reduced to Mo^{4+} atoms (10 electrons reduced) when discharge to 1.5 V, and also form two $[Mo_3^{IV}O_4]$ and two $[Mo_3^{IV}O_4py_3]$ units. Combining the original structure of **1** and Wang's

method[9], we also proposed the possible super reduced structure $[Sb_2Mo^{IV}_{12}O_{34}Py_6]^{14-}$ based on original structure Mo^{IV}_6-POM**1**.

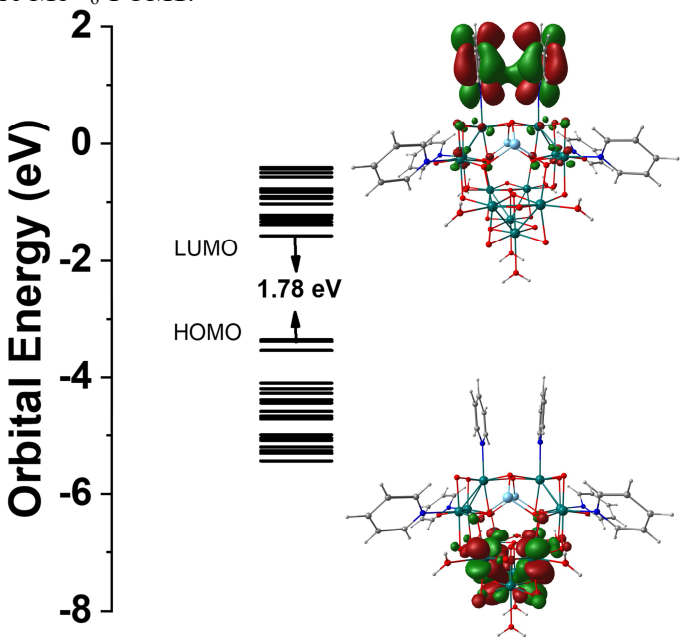

Figure S23. Representative molecule orbital and HOMO-LUMO gap of 24e-**1**.

S10-2 Electronic structure

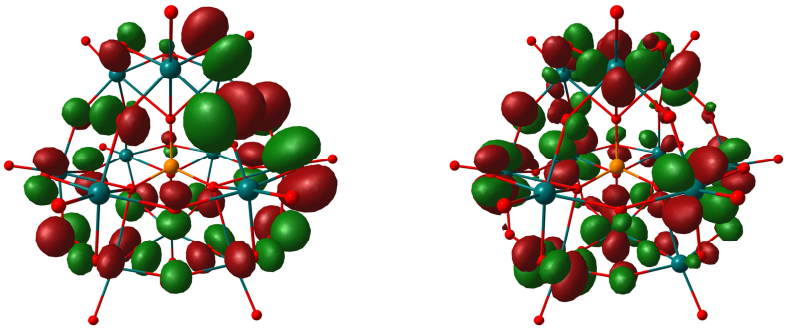

Figure S24. Representative molecular orbital of $[PMo^{VI}_{12}O_{40}]^{3-}$.

Table S9. Comparison of composition of HOMO and LUMO for PMo12 and Mo^{IV}_6-POM **1**-**3**.

Compound	HOMO (%)	LUMO (%)
PMo12	Mo^{6+}:6.5, O: 93.5	Mo^{6+}:73.6, O: 26.3
1	Mo^{4+}: 3.1, Mo^{5+}: 59.5, Mo^{6+}:3.5, O:33.1	Mo^{4+}: 24.1, Mo^{5+}: 10.2, Mo^{6+}:43.6, O: 20.4
2	Mo^{4+}: 2.0, Mo^{5+}: 61.3, Mo^{6+}:3.7, O:32.4	Mo^{4+}: 33.6, Mo^{5+}: 8.6, Mo^{6+}:37.3, O:19.4
3	Mo^{4+}: 61.7, Mo^{5+}: 0, Mo^{6+}:0.9, O:35.7	Mo^{4+}: 14.9, Mo^{5+}: 11.2, Mo^{6+}:48.7, O:22.8

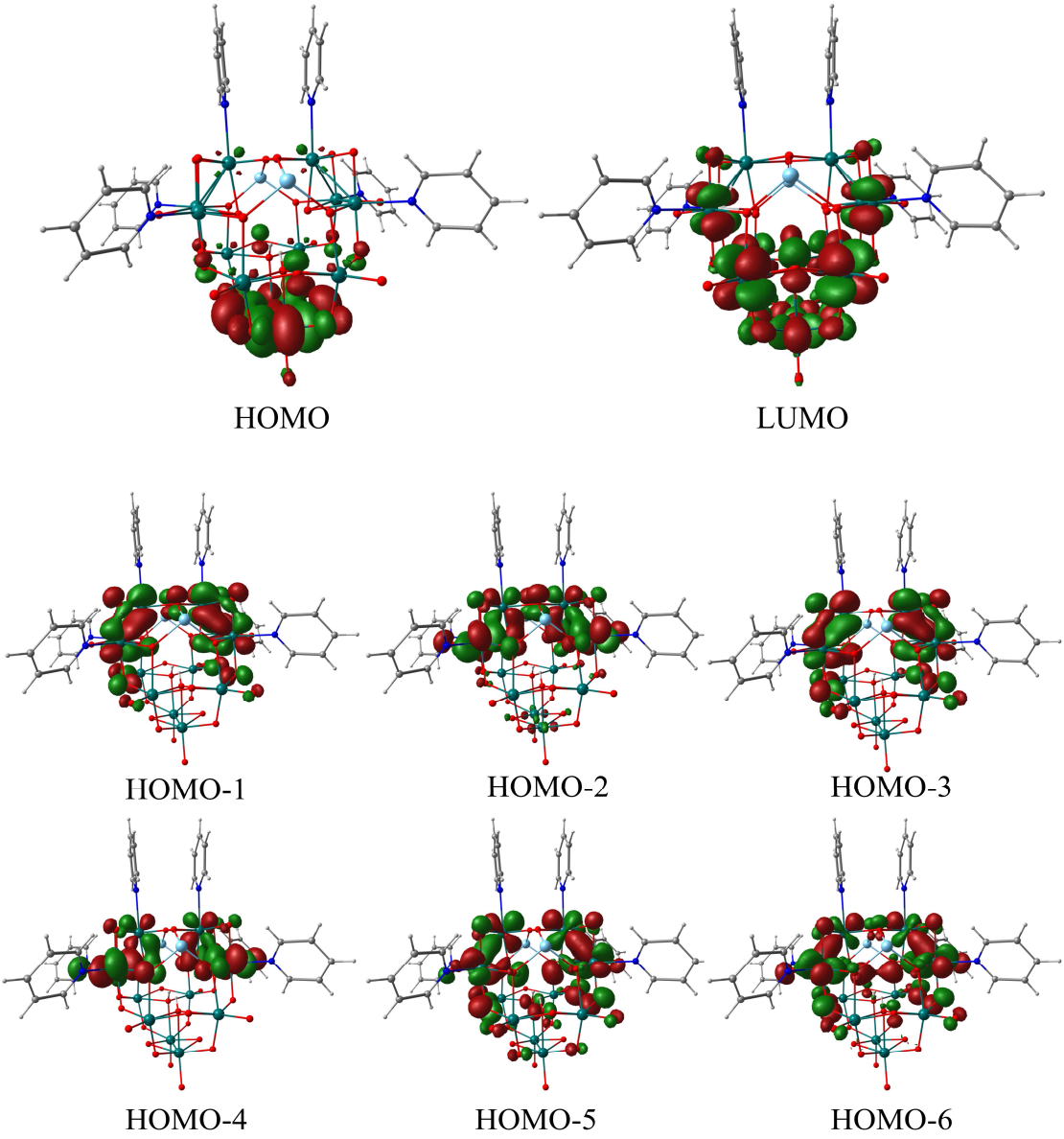

Figure S25. Representative molecular orbital of **1**.

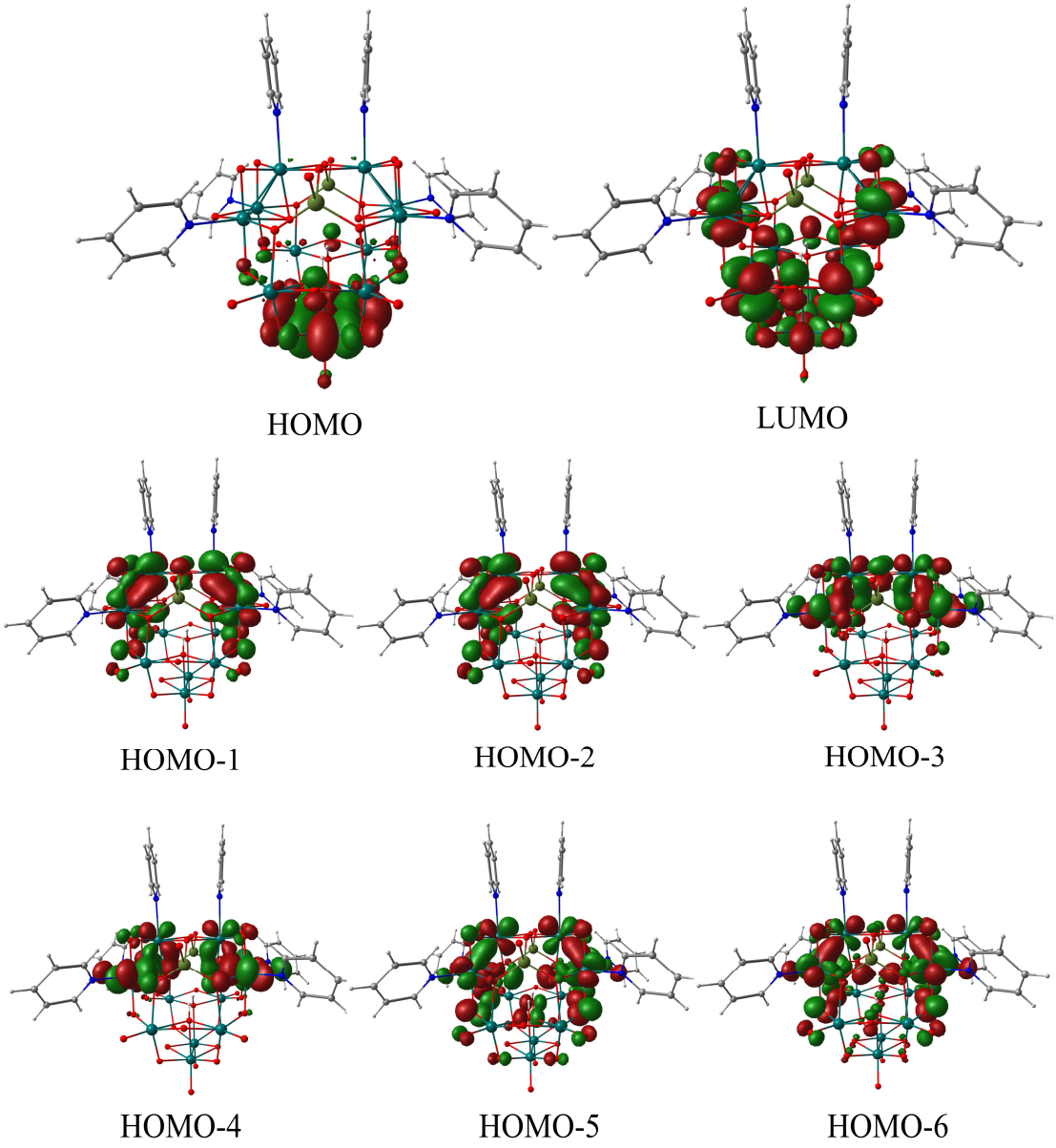

Figure S26. Representative molecular orbital of **2**.

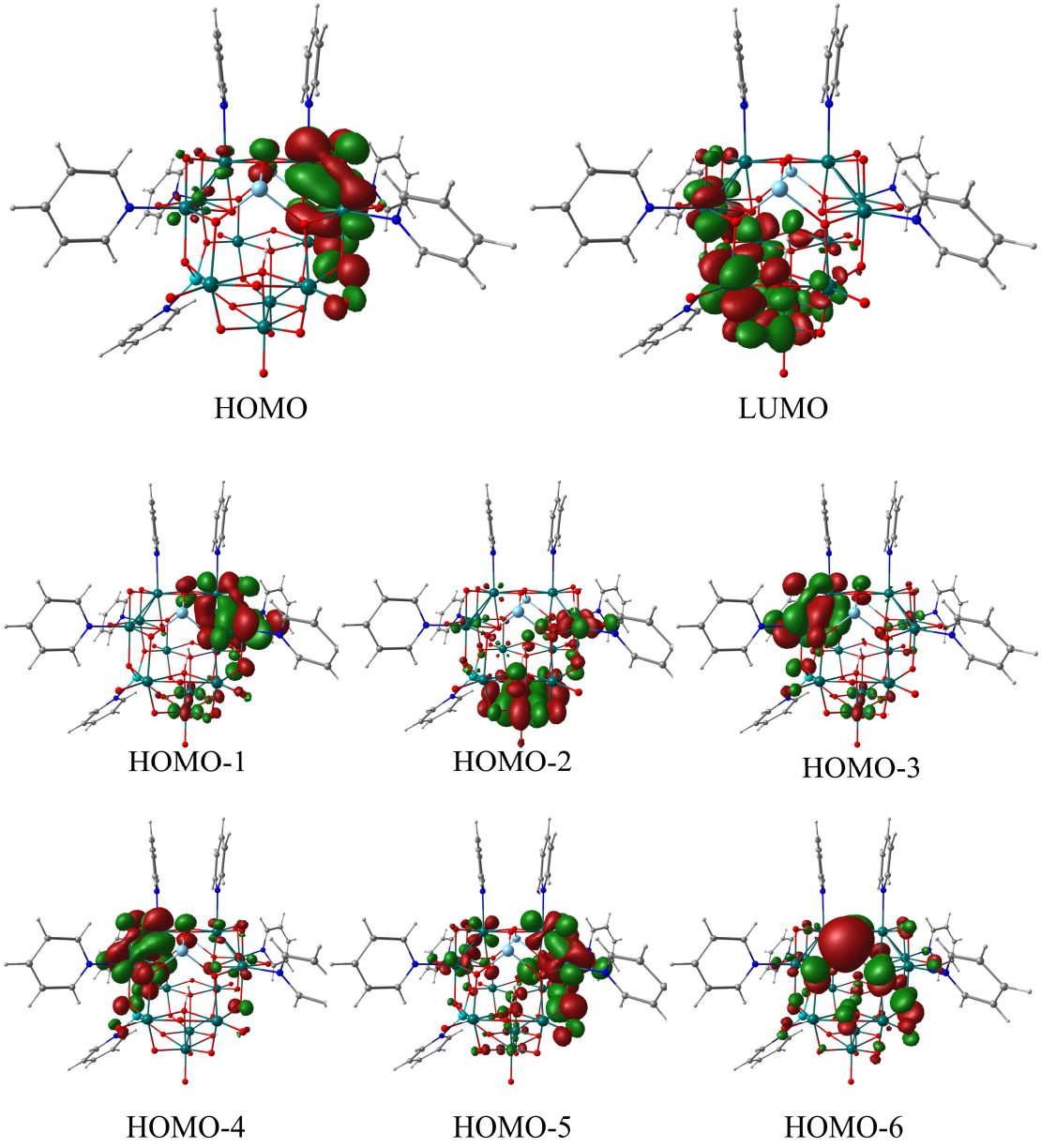

Figure S27. Representative molecular orbital of **3**.

Table S10. A comparison of metal Mulliken charge, Mo^{IV} charge transfer (Δ) and HOMO-LUMO gaps (eV) of Mo^{IV}_3-POMs **1**-**28** and related clusters.

Mo^{IV}_3-POMs	Mo^{IV}	Δ	M[a]	M[b]	Gap(eV)	ref.
6*e*-$[Mo^{IV}_3O_4(C_2O_4)_3(Mepy)_3]^{2-}$	1.217	0			3.44	5
12*e*-$[Sb^{III}_2Mo^{IV}_6Mo^{V}_2Mo^{VI}_4O_{32}(OH)_2py_6]^{2-}$ (**1**)	1.395	0.178	1.786 (Mo^{VI}), 1.605 (Sb^{III})	1.448 (Mo^{V})	2.90	this work
12e-$[(Ge^{IV}OH)_2Mo^{IV}_6Mo^{V}_2Mo^{VI}_4O_{32}(OH)_2py_6]^{2-}$ (**2**)	1.388	0.171	1.826 (Mo^{VI}), 1.935 (Ge^{IV})	1.450 (Mo^{V})	2.91	this work
12*e*-$[Sb^{III}_2Mo^{IV}_6Mo^{V}_2Mo^{VI}_4ZnO_{32}(OH)_2py_7]^{2-}$ (**3**)	1.438	0.221	1.828 (Mo^{VI}), 1.632(Sb^{III}),1.202 (Zn^{II})	1.511 (Mo^{V})	2.72	this work
12*e*-$[Mo^{IV}_3Mo^{V}_6Mo^{VI}_4O_{32}(OH)_2py_9]$ (**4**)	1.470	0.253	1.54(Mo^{V}_2), 1.79(•Mo^{V}),1.87(Mo^{VI})	1.94(Mo^{VI}),1.68(Mo^{V})	1.91	[27]
12*e*-$[Mo^{IV}_3Mo^{V}_6Mo^{VI}_4O_{32}(OH)(OMe)\ py_9]$ (**5**)	1.463	0.246	1.50(Mo^{V}_2), 1.78(•Mo^{V}),1.88(Mo^{VI})	1.95(Mo^{VI}),1.64(Mo^{V})	2.05	[27]
12*e*-$[Mo^{IV}_3Mo^{V}_6Mo^{VI}_4O_{32}(OH)(OEt)\ py_9]$ (**6**)	1.484	0.267	1.54(Mo^{V}_2), 1.81(•Mo^{V}),1.90(Mo^{VI})	1.95(Mo^{VI}),1.70(Mo^{V})	1.96	[27]
12*e*-$[Mo^{IV}_3Mo^{V}_6Mo^{VI}_4O_{32}(OH)(OPr)\ py_9]$ (**7**)	1.482	0.265	1.53(Mo^{V}_2), 1.73(•Mo^{V}),1.90(Mo^{VI})	1.90(Mo^{VI}),1.70(Mo^{V})	1.90	[27]
12*e*-$[Mo^{IV}_3Mo^{V}_6Mo^{VI}_4O_{32}(OH)(OCH_2H_4OH)\ py_9]$ (**8**)	1.466	0.249	1.53(Mo^{V}_2), 1.75(•Mo^{V}),1.90(Mo^{VI})	1.91(Mo^{VI}),1.69(Mo^{V})	1.97	[27]
11*e*-$[Mo^{IV}_3Mo^{V}_5Cr^{III}Mo^{VI}_4O_{32}(OH)_2py_{10}]$ (**9**)	1.467	0.250	1.53(Mo^{V}_2), 1.77(•Mo^{V}),1.87(Mo^{VI})	1.96(Mo^{VI}),1.03(Cr^{III})	2.47	[27]
12*e*-$[Mo^{IV}_3Mo^{V}_6Mo^{VI}W^{VI}_3O_{32}(OH)_2py_9]$ (**10**)	1.447	0.230	1.53(Mo^{V}_2), 1.77(•Mo^{V}),1.93(M^{VI})	2.11(M^{VI}),1.72(Mo^{V})	1.83	[27]
12e-$[Mo^{IV}_3Mo^{V}_6W^{VI}_4O_{33}(OH)\ py_9]^{-}$ (**11**)	1.453	0.236	1.54(Mo^{V}_2), 1.75(Mo^{V}),2.03 (W^{VI})	1.97(W^{VI}), 1.44(Mo^{V})	3.11	[27]
6*e*-$[Mo^{IV}_3Mo^{VI}W_8O_{30}(OH)_7py_3]^{2-}$ (**12**)	1.411	0.194	1.954(W^{VI})	2.168(W^{VI})	2.87	[21]
12*e*-$[Mo^{IV}_6W^{VI}_6O_{29}(OH)_5py_6]^{3-}$ (**13**)	1.335	0.118	1.938(W^{VI})	-	3.06	[21]
12*e*-$[Mo^{IV}_6W_6{}^{VI}O_{29}(OH)_5Na(H_2O)_5py_6]^{2-}$ (**14**)	1.346	0.129	1.982(W^{VI})	-	3.24	[21]
24*e*-$[(Mo^{IV}_6Mo^{VI}W_5{}^{VI}O_{28}(OH)_6)_2Znpy_{12}]^{2-}$ (**15**)	1.354	0.137	2.030(W^{VI})	-	3.19	[21]
12*e*-*γ*-$[Mo^{IV}_6Mo^{VI}_7O_{36}py_6]^{4-}$ (**16**)	1.069	-0.148	1.500(Mo^{VI})	1.306 (Mo^{VI})	2.99	[23]
12*e*-*β*-$[Mo^{IV}_6Mo^{VI}_7O_{36}py_6]^{4-}$ (**17**)	1.051	-0.166	1.535(Mo^{VI})	1.327 (Mo^{VI})	2.76	[7,23]
18*e*-$[Mo^{IV}_6Mo^{V}_6Mo^{VI}_9O_{58}py_6]^{8-}$ (**18**)	1.089	-0.128	1.207(Mo^{V}),1.374(Mo^{VI})	1.214(Mo^{V}),1.442(Mo^{VI})	1.91	[20]
36*e*-$[V^{IV}_2Mo^{IV}_{12}Mo^{V}_{12}Mo^{VI}_6O_{81}(OH)_2py_{12}]^{12-}$(**19**)	1.524	0.307	1.411(Mo^{V}),1.556(Mo^{VI})	-	0.79	[22]
36*e*-$[Mo^{VI}_2Mo^{IV}_{12}Mo^{V}_{12}Mo^{VI}_6O_{81}(OH)_2py_{12}]^{8-}$(**20**)	1.589	0.372	1.463(Mo^{V}),1.631(Mo^{VI})	-	0.67	[22]
28*e*-$[NaMo^{IV}_{12}Mo^{V}_4Mo^{VI}_3O_{44}py_{12}]^{-}$ (**21**)	1.032	-0.185	1.325(Mo^{V}),1.547(Mo^{VI}),1.579(Zn^{II})	-	1.48	[10]
6*e*-$[ZnMo^{IV}_3Mo^{VI}_{10}P_4O_{49}py_3]^{4-}$ (**22**)	1.189	-0.027	1.601(Mo^{VI}), 1.436(P^{V})	1.659(Mo^{VI})	0.71	[10]
6*e*-$[Sb_3Mo^{IV}_3Mo^{VI}_{15}O_{57}py_3]^{3-}$ (**23**)	1.462	0.245	1.889(Mo^{VI})	1.942(Mo^{VI}),1.706(Sb^{III})	0.77	[24]
12*e*-$[Mo^{IV}_6Mo^{VI}_{10}Ge_3O_{48}py_6]$ (**24**)	1.192	-0.025	1.551(Mo^{VI}), 1.617(Ge^{IV})	1.579(Mo^{VI})	0.48	[20]
1D-12*e*-$[Mo^{IV}_6Mo^{VI}_4Ge_2O_{30}py_6]^{4-}$ (**25**)	1.331	0.114	1.684(Mo^{VI}), 1.691(Ge^{IV})	1.918(Mo^{VI})	3.18	[26]
2D-6*e*-$[Mo^{IV}_3Mo^{VI}_9P_7Zn_4O_{56}py_3]^{3-}$ (**26**)	1.526	0.309	2.314(P^{V}), 1.261(Zn^{II})	1.918(Mo^{VI})	0.36	[26]

[a] Mo^{IV}-$\mu_{2,3}$-O-M. [b] M': not linked to Mo^{IV} by $\mu_{2,3}$-O.

Table S11. The cartesian coordinates of 24e-**1** (in Å)

Mo	-2.90867027	0.39658434	-1.27955245
Mo	-1.66219006	2.24325935	-0.14935831
N	-4.50011046	0.34723648	-2.80669584
Mo	-2.90202017	0.56710965	1.21629826
O	-2.87501021	2.27212942	-1.67142318
O	-1.35068011	0.22209824	-0.01597154
O	-2.79140036	-1.72432531	-1.39545570
O	-1.61438026	-0.07664708	-2.75333998
O	-4.40149034	0.23314831	0.00917837
N	-1.70013998	4.43112532	-0.28641701
O	0.00000013	2.55732967	1.01247936
O	0.00000002	2.30940502	-1.29873060
O	-2.95648009	2.49279344	1.23275417
C	-5.61495056	-0.45554025	-2.59052120
C	-4.38648047	1.07853303	-3.98409395
O	-1.62296002	0.33596016	2.67915579
O	-2.82356022	-1.50612328	1.68137861
N	-4.50868022	0.68827552	2.71618145
Mo	-1.24498031	-2.08184832	-2.77969604
Sb	-0.00000009	1.05059655	-2.85249209
C	-1.67227001	5.05986171	-1.52458858
C	-1.80947991	5.18314964	0.87651899
Mo	1.66219020	2.24325922	-0.14935845
Sb	0.00000015	1.45495803	2.68199398
H	-5.69267056	-0.95262205	-1.78517175
C	-6.61617069	-0.52701300	-3.55173262
C	-5.38770058	1.00254390	-4.94636940
H	-3.62590040	1.62566801	-4.13202509
Mo	-1.24348005	-1.65806725	3.04024248
C	-4.47867014	1.63526123	3.73491996
C	-5.57636036	-0.19500986	2.62041786
Mo	-0.00000023	-3.76096235	-1.42253617
Mo	1.24497988	-2.08184842	-2.77969614
O	-0.00000027	-1.95245173	-4.28407779
O	-0.00000013	-1.77841644	-1.10686965
O	-1.47717040	-4.02475585	-2.68070395
O	-2.81712050	-2.17607388	-4.31474946
O	1.61437999	-0.07664720	-2.75334011
H	-1.59789005	4.54461077	-2.31873129
C	-1.75587996	6.44497815	-1.60050466
C	-1.89308987	6.56811235	0.79882920
H	-1.82865990	4.75303655	1.72235490
Mo	2.90867017	0.39658411	-1.27955268

Mo	2.90202028	0.56710942	1.21629803
N	1.70014028	4.43112518	-0.28641715
O	2.87501023	2.27212920	-1.67142342
O	1.35068010	0.22209813	-0.01597165
O	2.95648036	2.49279320	1.23275392
O	1.62296023	0.33596003	2.67915566
H	-7.37784075	-1.07531494	-3.40403795
C	-6.50254073	0.20428123	-4.72912100
H	-5.31109058	1.50297049	-5.75087185
O	-2.78925010	-1.49942143	4.61435393
Mo	1.24348014	-1.65806735	3.04024238
Mo	-0.00000008	-3.51710455	1.92027507
O	-0.00000002	-1.48050933	1.37042523
O	0.00000012	-1.35596515	4.53759805
O	-1.47931014	-3.65282327	3.19256373
H	-3.74823006	2.23981111	3.79974047
C	-5.51419019	1.69459147	4.65859253
C	-6.61188039	-0.13567961	3.54409043
H	-5.59643042	-0.84152982	1.92456580
O	-0.00000031	-5.99487009	-1.32155137
O	-1.33567026	-3.76469638	0.31946570
O	1.33566995	-3.76469649	0.31946559
O	1.47716983	-4.02475596	-2.68070407
O	2.79140007	-1.72432554	-1.39545594
O	2.81711993	-2.17607411	-4.31474969
H	-1.73810998	6.87688336	-2.44700384
C	-1.86735989	7.20136278	-0.43826862
H	-1.96887982	7.08531839	1.59404343
N	4.50011022	0.34723612	-2.80669622
O	4.40149033	0.23314796	0.00917801
O	2.82356021	-1.50612351	1.68137837
N	4.50868047	0.68827516	2.71618108
C	1.67227025	5.05986158	-1.52458872
C	1.80948036	5.18314949	0.87651884
H	-7.18705076	0.15248990	-5.38688083
O	2.78925033	-1.49942165	4.61435370
O	1.47931008	-3.65282339	3.19256361
O	-0.00000016	-5.77659050	2.05675421
H	-5.49436012	2.34113317	5.35422361
C	-6.58187032	0.81129636	4.56282663
H	-7.34253044	-0.74025132	3.47905916
H	-1.92361986	8.14723346	-0.49062251
C	5.61495030	-0.45554069	-2.59052166
C	4.38648019	1.07853268	-3.98409431

C	4.47867054	1.63526087	3.73491959
C	5.57636052	-0.19501031	2.62041740
H	1.59789019	4.54461064	-2.31873142
C	1.75588031	6.44497799	-1.60050481
C	1.89309042	6.56811219	0.79882904
H	1.82867038	4.75303641	1.72235474
H	-7.29148034	0.85111284	5.19388042
H	5.69267029	-0.95262251	-1.78517222
C	6.61617032	-0.52701353	-3.55173317
C	5.38770021	1.00254348	-4.94636985
H	3.62590015	1.62566772	-4.13202539
H	3.74823052	2.23981081	3.79974015
C	5.51419066	1.69459104	4.65859207
C	6.61188065	-0.13568014	3.54408988
H	5.59643047	-0.84153027	1.92456534
H	1.73811029	6.87688325	-2.44700399
C	1.86736040	7.20136267	-0.43826878
H	1.96888048	7.08531823	1.59404326
H	7.37784038	-1.07531553	-3.40403856
C	6.50254030	0.20428071	-4.72912154
H	5.31109021	1.50297007	-5.75087228
H	5.49436070	2.34113273	5.35422318
C	6.58187069	0.81129584	4.56282608
H	7.34253065	-0.74025190	3.47905855
H	1.92362044	8.14723330	-0.49062267
H	7.18705034	0.15248933	-5.38688141
H	7.29149077	0.85111226	5.19387982
H	-0.73449038	-6.42491984	-1.17079854
H	0.73448973	-6.42491989	-1.17079859
H	0.71688988	-6.22436463	2.11482964
H	-0.71689023	-6.22436458	2.11482970
H	-3.46459017	-2.04837915	4.62129617
H	-2.71021004	-0.90068218	5.23537770
H	3.46459036	-2.04837943	4.62129588
H	2.71021037	-0.90068240	5.23537748
H	-3.49782057	-2.70506896	-4.20669288
H	-2.72734050	-1.72757704	-5.05374086
H	2.72733991	-1.72757726	-5.05374109
H	3.49781997	-2.70506923	-4.20669317

References

1. A. Bino, F. A. Cotton and Z. Dori, *J. Am. Chem. Soc.*, 1978, **100**, 5252-5253.
2. S. F. Gheller, T. W. Hambley, R. T. C. Brownlee, M. J. O'Connor, M. R. Snow and A. G. Wedd, *J. Am. Chem. Soc.*, 1983, **105**, 1527-1532.
3. K. Tang, X. Q. Yu, J. P. Sun, H. Li and X. J. Huang, *Electrochim. Acta*, 2011, **56**, 4869-4875.
4. R. Tsunashima, Y. Iwamoto, Y. Baba, C. Kato, K. Ichihashi, S. Nishihara, K. Inoue, K. Ishiguro, Y. F. Song and T. Akutagawa, *Angew. Chem. Int. Ed.*, 2014, **53**, 11228-11231.
5. B. Modec and P. Bukovec, *Inorg. Chim. Acta*, 2015, **424**, 226-234.
6. H. Yoshikawa, C. Kazama, K. Awaga, M. Satoh and J. Wada, *Chem. Commun.*, 2007, DOI: 10.1039/B707189B, 3169-3170.
7. H. Wang, T. Yamada, S. Hamanaka, H. Yoshikawa and K. Awaga, *Chem. Lett.*, 2014, **43**, 1067-1069.
8. S. Uematsu, Z. Quan, Y. Suganuma and N. Sonoyama, *J. Power Sources*, 2012, **217**, 13-20.
9. A. D. Becke, *J. Chem. Phys.*, 1993, **98**, 5648-5652.
10. M. J. Frisch, G. W. Trucks, H. B. Schlegel, G. E. Scuseria, M. A. Robb, J. R. Cheeseman, G. Scalmani, V. Barone, G. A. Petersson, H. Nakatsuji, X. Li, M. Caricato, A. V. Marenich, J. Bloino, B. G. Janesko, R. Gomperts, B. Mennucci, H. P. Hratchian, J. V. Ortiz, A. F. Izmaylov, J. L. Sonnenberg, Williams, F. Ding, F. Lipparini, F. Egidi, J. Goings, B. Peng, A. Petrone, T. Henderson, D. Ranasinghe,

V. G. Zakrzewski, J. Gao, N. Rega, G. Zheng, W. Liang, M. Hada, M. Ehara, K. Toyota, R. Fukuda, J. Hasegawa, M. Ishida, T. Nakajima, Y. Honda, O. Kitao, H. Nakai, T. Vreven, K. Throssell, J. A. Montgomery Jr., J. E. Peralta, F. Ogliaro, M. J. Bearpark, J. J. Heyd, E. N. Brothers, K. N. Kudin, V. N. Staroverov, T. A. Keith, R. Kobayashi, J. Normand, K. Raghavachari, A. P. Rendell, J. C. Burant, S. S. Iyengar, J. Tomasi, M. Cossi, J. M. Millam, M. Klene, C. Adamo, R. Cammi, J. W. Ochterski, R. L. Martin, K. Morokuma, O. Farkas, J. B. Foresman and D. J. Fox, *Gaussian, Inc., Wallingford CT,* 2009.

11. P. J. Stephens, F. J. Devlin, C. F. Chabalowski and M. J. Frisch, *J. Phys. Chem.*, 1994, **98**, 11623-11627.

12. P. J. Hay and W. R. Wadt, *J. Chem. Phys.*, 1985, **82**, 299-310.